Empirical mode decomposition based approach to the detection of decompression induced gas bubbles in the blood vessel from pulsed Doppler ultrasound signal

THESIS

Empirical mode decomposition based approach to the detection of decompression induced gas bubbles in the blood vessel from pulsed Doppler ultrasound signal

MD IQBAL AZIZ KHAN

Department of Information Science and Technology

Graduate School of Science and Technology, Educational Division, Shizuoka University

June 2015

DEDICATED TO MY INNOCENT FATHER

Abstract

This thesis concerns the detection of decompression induced gas bubbles in the flowing blood. Gas bubbles are a major clinical issue often encountered in the pneumatic caisson, flying, scuba diving and medical fields. Presenting a significant health hazard, these gas bubbles could occlude blood vessels and thereby prevent the normal flow of blood to surrounding tissue and vital organs. As a result, it can lead to momentary neurological deficits up to heart attack and stroke. It is believed that detecting the gas bubbles in the early stage could prevent or reduce the gas bubbles associated risks. The signal analyzed in this thesis is collected targeting the pulmonary artery of caisson workers who are infected due to decompression; using the pulsed Doppler ultrasound system. Doppler ultrasound signal is graded from low to high. Some simple algorithms are required to the detection of gas bubbles for low graded Doppler ultrasound signal. However gas bubble detection is challenging if the signal belongs to high grade. In this thesis gas bubble detection is carried out for low graded Doppler ultrasound signal as well as high graded Doppler ultrasound signal.

This signal is decomposed into its individual embedded modes called intrinsic mode functions (IMF) with the empirical mode decomposition (EMD) method. Then discrete Hilbert transform (DHT) is applied to the disintegrated intrinsic mode functions (IMF) subsequently to generate the three time-dependent instantaneous components-

frequency, Hilbert amplitude and phase. The EMD combined with DHT constitutes the Hilbert spectrum (HS) which is a fine-resolution time-frequency-energy representation of a non-stationary signal. Therefore, the HS is generated from the normalized instantaneous frequencies and weighted sum of instantaneous amplitudes of the IMFs at the frequency bins. A new representation and interpretation of Doppler ultrasound signal is given to the time-frequency-energy distribution using HS. In the new representation of HS, a search area with parabolic outline is found within which it is expected that the systolic phase and the gas bubble signal exists. This search area appears clearly due to the strength of the systolic phase and the gas bubble signal. The systolic phase is detected by deriving the ratio between high frequency components and low frequency components and using the instantaneous phase through the reconstruction of the signal. Detecting systolic phase or peak systole could provide the cardiac rate variability as well as tentative location of the gas bubble signal. Then, systolic phase detection performance is evaluated in terms of sensitivity and positive predictivity. More processing steps are required to isolate the gas bubble signal.

In the next step, time-varying mean frequency domain and IMF-based time domain analysis of Doppler ultrasound signal is employed to extract the gas bubble signal. This time-varying mean frequency is derived using the instantaneous frequency (IF) and the instantaneous amplitude, which is a very useful curve. Some smooth rising

trends or segments are figured out in this curve which could belong to the gas bubble signal. These segments are examined to see if their proximity to the gas bubble signal characteristics is compatible. At first the segments are extracted by applying the ascending slope tracing algorithm on the basis of segments amplitude, average slope and the deflection width. In addition, these segments corresponding sections in the IMFs are extracted and combined. A number of features or parameters are defined for the segments in time-varying mean frequency domain. Similarly, another set of parameters are defined for the segments in IMF-based time domain. Taking into account the gas bubble signal characteristics, thresholds are determined from all the segments. Utilizing these thresholds and the parameter values, a set of fuzzy logic based rules are proposed for each of the parameters. Consequently membership values are determined for all the parameters of a segment. Then average membership value is calculated from the membership values. Three kinds of detection results are illustrated, “detected”, “detected with poor accuracy” and “not detected”, on the basis of the average membership value. The proposed algorithm is applied to a subset of the available database and appears to perform with good sensitivity even when the gas bubble signal has variable signal strength and duration.

Acknowledgements

This work is carried out in the Department of Information Science and Technology, Graduate School of Science and Technology, Shizuoka University, Japan.

This work would not have been possible without the help of many people. First, I am very thankful to my supervisor, Dr. Takayoshi Nakai, for his precious support and mentorship, which has kept me on the right track during the full duration of my PhD degree. The time spent under his supervision has been the most productive in my academic life. His expertise in the area of Digital Signal Processing and diligence in research have motivated me to self-improve. I wish to appreciate his outstanding guidance and insightful instructions that were invaluable in the completion of my thesis.

My mother, father, mother-in-law, father-in-law, sisters and brother-in-laws– this is for you. This is for what you believed I was capable of. This is for the arms that carried me through so many dark hours of self-doubt and confidence conflicts through my life this far. I am nothing without your unshakeable faith in me, your unconditional love and support. I am so blessed.

I would like to thank Dr. Md. Ekramul Hamid, Dr. Xin Dang, Dr. Shamim Ahmad, Dr. Earfan Hamid and Dr. Md. Khademul Islam Molla for serving as an advisor throughout my doctoral program and for sharing their expertise. I would also thanks to all lab members for their helpful suggestions and encouragements in this research. With their companionship, I have learned a lot and enjoyed Japan very much.

My friends – old and relatively new and its loo long a list to name, so I won't. I am so grateful to each of you for everything you have brought to my life for being there during some really tough times and more, for the fun times. I am here in many ways because of you all. I won't thank you for your companionship or the shoulders that I have used too often to account for. In too many ways it's a blessing and I'm only immensely grateful.

My wife Nayeem and my baby Ohee – this is for you. I am deeply indebted to my family and most of all to my wife for her sacrifice, love and support.

The author would like to thank Mr. Tohru Mochizuki, Diving Technology Center Company Limited, Tokyo, Japan for providing the Doppler ultrasound signals and some important resources. The signals containing gas bubbles are used to test my algorithm.

Mr. Keizo Ishida – a special thank you. For all the help – and that's been quite a bit which you have always extended without the least bit of hesitation. You have been an inspiration. Thank you.

The author would like to acknowledge the financial support provided by the Japan government through MEXT scholarship. Thanks to all staff of the Graduate School of Science and Technology, Shizuoka University and University Library for their kind cooperation. Also thanks to the authority of Rajshahi University, Bangladesh for granting me the study leave.

Contents

List of figures

List of tables

CHAPTER 1

Introduction to decompression induced gas bubble

1.1 Introduction

An embolus is defined as an abnormal particle entrained within the bloodstream [1]. An embolus could be a gas bubble [2], a fat globule [3], a blood clot, tumor tissue, platelet aggregate, an athermanous plaque or a piece of a thrombus [4][5][6]. The plural of embolus is emboli. A single or multiple emboli can result in a sudden interruption of blood flow to an organ or body part is called embolism. Important variations are found in the nature, the size and the number of emboli on the basis of clinical situation. Obstruction of a blood vessel could be caused by either a large gas bubble or a set of small gas bubble. A moving gas bubble in the blood vessel is shown in Fig. 1.1.

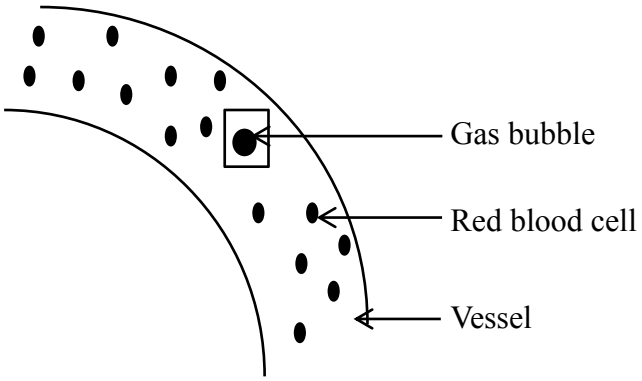

Fig. 1.1: A moving gas bubble in the blood vessel

1.2 Sources of gas bubble

Gas bubble or embolus is reported in a wide variety of clinical fields. The two most common sources for gas bubbles are as a result of a medical procedure and through

environmental decompression [7]. Gas bubbles concerning medical procedures are not discussed in this research. Environmental decompression is observed while carrying out construction, maintenance or other works in the pneumatic caisson, flying and scuba diving. Pneumatic caisson is used during the construction work such as foundation work, i. e., basements and shafts of the bottom tunnel or shields for subway and so forth [8]. A simple diagram of a pneumatic caisson is illustrated in Fig. 1.2.

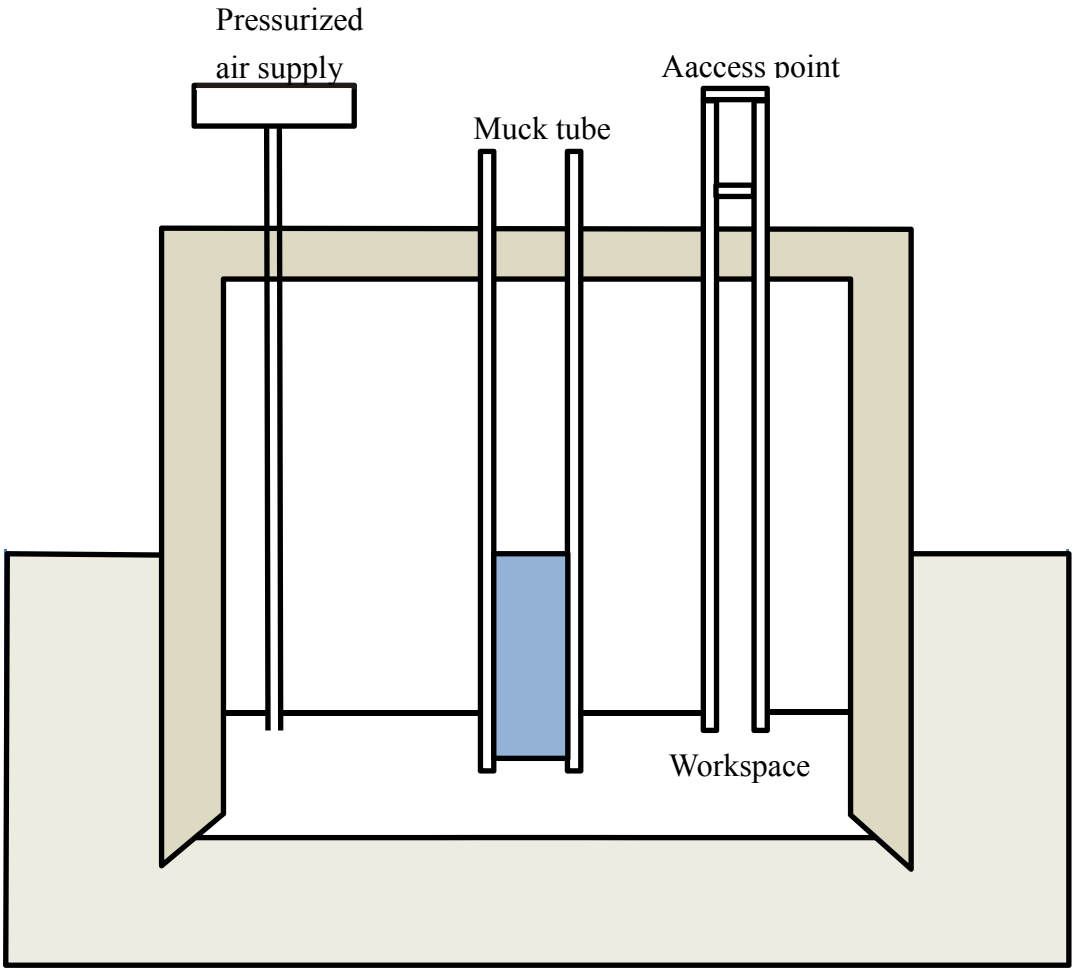

Fig. 1.2: A simple diagram of a pneumatic caisson

In this system, the workers are exposed to hyperbaric environments where compressed air is maintained, even though this system has risks to be suffered from not

only decompression sickness but also poisonous gas toxicity or organ deficiency. However, this caisson work is considered as a better technique for such high pressure works, even though the workers must be exposed to hyperbaric working environments for maintenance or repair of machineries and materials.

In this system, mixed gas of oxygen, helium and nitrogen (Trimix) is used for breathing through masks instead of air at the bottom working fields. Unlike oxygen, nitrogen and helium is a biologically inert gas, meaning that it is not converted into other substances by the body. For this reason, most of the nitrogen we inhale is expelled when we exhale, but some is dissolved into the blood and other tissues. During the construction work, however, the lungs take in more nitrogen than usual. This happens because the surrounding pressure is greater than air pressure at sea level. When the environmental pressure decreases by surfacing, the gas that is absorbed in tissue becomes gas bubbles and is evacuated out of body through several paths. If the generation speed of the bubbles is slower than the evacuation speed, there is no problem. In rapid surfacing, however, the generation speed is increased above that of evacuation and the bubbles remaining in the body could block small vessels or compress nerves, and result in various functional disorders. Such disorders are called decompression disorders or caisson disease. Caisson disease is named after the caissons or large underwater chambers in which underwater construction workers often worked. During

decompression bubbles are present in varying quantities. Large quantities of bubbles are believed to be harmful to the body and are generally considered the initiating factor for decompression sickness. The risk of developing decompression sickness is correlated with gas bubble grades.

1.3 Disease due to gas bubble

A number of terms are used to describe the decompression disorders. Decompression sickness, decompression illness, decompression injury, bends and caisson disease are all used to describe the same condition.

1.3.1 Decompression sickness of the nervous system

The clinical features are due to disturbance of activity in the nervous system, interfering with one or more of its five principal functions and could originate from the central, peripheral or autonomous nervous systems [9]. The symptoms appear a short time after the event that has led to the formation of gas bubbles. The neural status shows mostly multifocal lesions, and if the brain is affected, confusion, vertigo, unconsciousness, and disturbances of vision are preeminent. Disturbances of motility and of sensation and paralyses, including disturbances of micturition, are symptoms of damage to the spinal cord. Damage to the inner ear is indicated by some features such as ringing noises in the ears (tinnitus), loss of hearing, vertigo and vomiting. The increase of concentration in high pressure air increases the tracheal resistance and in the worst case gas bubbles are

carried by the systemic circulation to the lungs, pulmonary symptoms ensue facultatively, with dyspnea, cyanosis, pain in the chest upon breathing and somewhat bloody expectoration.

1.3.2 Decompression sickness of the skin, muscles, bones and joints

The cause of this decompression sickness is the presence of gas bubbles in the organs as a consequence of inadequate decompression. The exact location of these gas bubbles and the mechanisms causing pain are not very clear. Decompression sickness of the skin exhibits itself with itching, red spots, and swellings. Stiffness of the muscles and soreness after sudden and protracted exercise indicates damage to the muscles. Symptoms due to decompression sickness of the joints are often found around a joint. Symptoms could begin with discomfort or an abnormal feeling in or near the joint. Over the next hour or two, pain and other symptoms could be developed. In comparison with the central nervous system, the bones and joints require little blood and the equalization of blood with that of the insert gas occurs very slowly. This is why the sickness affects the professional caisson workers adversely, who are exposed to overpressures for hours or even days.

1.3.3 Pulmonary decompression sickness

Pulmonary decompression sickness is another condition. The small vessels of the lungs could be trapped due to the formation of large number of gas bubbles. If excessive bubbles are formed, this leads to a disturbance of lung function and a feeling of breathlessness, known as the “chokes” [10]. Chokes are characterized by the triad of substernal pain, cough, and dyspnea, are considered to be associated with severe accumulation of gas bubbles and could rapidly develop into a life-threatening medical emergency [9].

1.4 Spencer code

The most common method for identification of bubbles in Doppler signals by listening and estimating the number of bubble signals according to some classification scheme. The Spencer code, proposed by M.P. Spencer is the first standard code for classifying gas bubbles [11]. He developed a scale to describe the rate and size of gas bubbles. It is illustrated in Table 1.1.

Table 1.1: Spencer code for gas bubble signals

Grade	Description
0	There is no gas bubble in the bloodstream
I	Occasional gas bubbles are detected and most of the cardiac periods are free from gas bubbles
II	Less than half of the cardiac periods contain single or multiple gas bubble signals in group
III	Most of the cardiac periods contain single or multiple gas bubble signals in group provided that the cardiac motion signal is still audible.
IV	The maximum detectable gas bubble signals sounding continuously throughout the every cardiac periods and overriding the amplitude of the cardiac motion signals.

1.5 Doppler ultrasound systems

The Doppler ultrasonic flowmeter is the simplest application of ultrasound for bubble detection. Doppler ultrasound is based on the shift of frequency in an ultrasound wave caused by a moving reflector, such as gas bubble or blood cell [12]. Reflected ultrasound waves are shifted in frequency proportionally to the velocity of a moving

reflector. This change in frequency is called the Doppler shift, and is given by

$$\Delta f = \frac{2\, f v\, cos\theta}{c}, \tag{1.1}$$

where f is the frequency of the transmitted signal, v is the velocity of the reflector, θ is the angle between the transmitted signal and the direction of the moving reflector and c is the sound velocity. It is illustrated in Fig. 1.3.

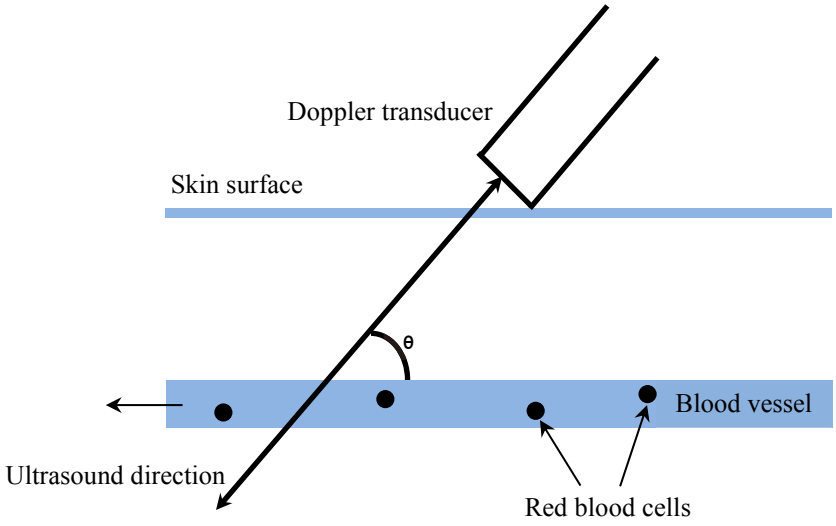

Fig. 1.3: Doppler ultrasound signal reflection into blood vessel

The Doppler shift typically falls in the audible range 0-10 kHz and is simply used as audible output. So the output Doppler signal is a sound with frequency proportional to the velocity of the reflectors and amplitude according to their acoustic properties. Reflections from stationary structures will not have a Doppler shift and will thus not be heard in the output signal. Any gas bubble moving with the blood flow will give very strong reflections that could be distinguished from the low amplitude flow

signal from blood cells.

Doppler ultrasound systems can be either continuous wave (CW) or pulsed wave (PW) [13]. In a CW system there are two transducers; one continuously transmitting ultrasound waves and one continuously receiving reflections. An oscillator generates a resonant frequency to drive the transmit transducer and provides the same frequency signal to the demodulator, which compares the returning frequency to the incident frequency. The receiver amplifies the returning signal and extracts the residual information containing the Doppler shift frequency by using a low-pass filter. CW systems are technically simpler and cheaper than PW systems, and also easier to use. They are therefore the most commonly used for the detection of gas bubbles. However, CW Doppler suffers from depth selectivity with accuracy affected by object motion within the beam path.

A PW Doppler system comprises a single transducer which emits short bursts of ultrasound and then “listens” for echoes. As the sound velocity in the tissue is known, one can define the depth from which to receive echoes by adjusting the time delay from transmission to reception and the duration of reception. Thus, PW Doppler systems have depth resolution which can improve the signal to noise ratio. It can be considered a depth-selective version of CW Doppler, returning information about the depth of reflectors in addition to their size and velocity. However, if the sample volume is not

optimally adjusted, part of the blood flow will be lost. Fig. 1.4 illustrates a simple block diagram of the pulsed Doppler ultrasound system.

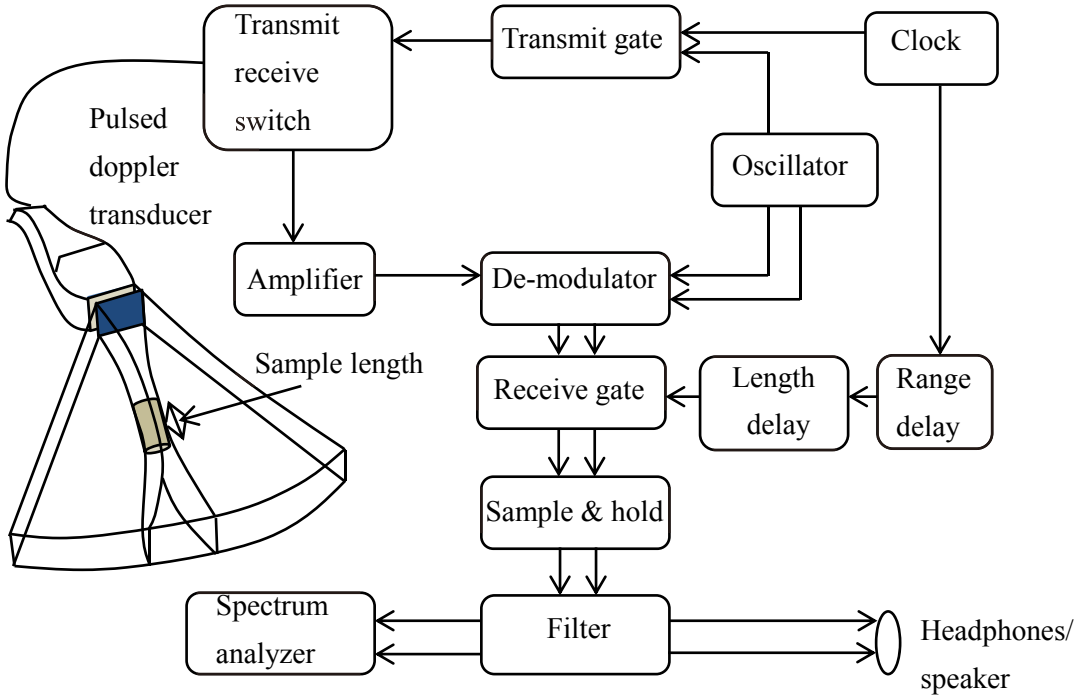

Fig. 1.4: Block diagram of a pulsed Doppler ultrasound system

Each Doppler pulse does not contain enough information to completely determine the Doppler shift, but only a sample of the shifted frequencies measured as a phase change. Stationary objects within the sample volume do not generate a phase change in the returning echo when compared to the oscillator phase, but a moving object does. Repeated echoes from the active gate are analyzed in the sample and hold circuit, and a Doppler signal is gradually built up.

Most ultrasonic scanners used for 2-dimensional imaging also have both CW and PW Doppler functions for blood flow measurements. This enables the operator to

easily find an optimal position for the Doppler signal and to avoid fast moving structures like valve cusps. Ultrasound scanners are, however, expensive and complex pieces of equipment and their use has so far been limited to laboratory experiments.

1.6 Experimental setup

A pulsed wave (PW) Doppler system comprises a single transducer which emits short bursts of ultrasound and then “listens” from echoes. In our research, a PW Doppler system having 2 MHz carrier frequency is used. Doppler ultrasound signal is radiated targeting the pulmonary artery and the reflected signal is received. The reflected signal is a sound with frequency proportional to the velocity of the reflectors and amplitude according to their acoustic properties. Reflections from moving objects (blood, gas bubble) will have a Doppler shift and will be found in the output signal and the Doppler signal is obtained by bandpass filtering through hardware.

1.7 Organization of the thesis

This opening chapter serves as an introduction to gas bubble, how gas bubble forms in the blood vessel, different disease due to gas bubble, gas bubble classification scheme, and Doppler ultrasound systems for the detection of gas bubbles. Below is an organization of the thesis in chapter-by-chapter basis.

Chapter 2

A comprehensive review of the gas bubble detection approaches are discussed in this chapter. Different types of gas bubble detection methods, their usefulness, effectiveness, and limitations are also discussed.

Chapter 3

Systolic phase detection approach based on EMD, DHT and HS is discussed in this chapter. How systolic phase detection is playing a vital role to the detection of gas bubble signal is discussed in the chapter. Some experimental results for the detection of systolic phase are given. In addition to this, decomposing a Doppler ultrasound signal into IMFs using EMD, determination of IF, instantaneous amplitude and instantaneous phase by DHT, and derivation of HS and a new representation of HS is given in the chapter.

Chapter 4

Derivation of time-varying mean frequency from instantaneous frequency and instantaneous amplitude is given in this chapter. An algorithm is proposed in this chapter for extracting the segments from the time-varying mean frequency. These segments are representing either gas bubble signal or other similar events.

Chapter 5

The segments extracted in the previous chapter are used in this chapter to define some parameters in time-varying mean frequency domain. In addition to this, some parameters are defined in time domain using IMFs. The segment representing gas bubble or not is determined on the basis of these parameters.

Chapter 6

Having obtained all the parameters in time-varying mean frequency and time domain, an algorithm based on fuzzy logic rule is applied for the purpose of gas bubble detection.

Chapter 7

This chapter summarizes the main conclusions of this thesis and provides some suggestions for further research.

CHAPTER 2

Literature review

2.1 Focus of the past and current research

Studies of embolic signal have mainly focused on the detection and discrimination using various methods and signal processing approaches. The earliest method of detection, which is still currently the gold standard, is that involving human experts. Automatic detection algorithms that have been developed operate either in the time domain or employ spectral techniques. Time domain based methods have used signal properties such as magnitude and instantaneous frequency of the signal. Spectral methods have allowed utilization of signal properties like intensity and frequency to distinguish between background and the embolic signal. Extensive research was carried out for the analysis of embolic signals. In the following sections, some well-known and effective methods are discussed.

2.1.1 FFT-based methods

Emmanuel Roy, Silvio Montresor, Pierre Abraham, and Jean-Louis Saumet presented a time-frequency representation based on the spectrogram to perform automatically the detection of circulating embolus [14]. The method used the narrow band hypothesis and extracted two characteristic functions from the time-frequency (TF) representation, the root-mean of the local power spectrum (RMPS) and the modal frequency (the frequency

for which the peak spectral power is maximum) for the detection of embolic signals. This method employed STFT for TF representation of the embolic signal. The representation efficiency depends on many factors including the number of FFT points, window function and amount of overlapping. Moreover, STFT introduces a remarkable amount of cross-spectral terms between the time frames. In addition to this, authors specified that their Doppler signals were less complex than those found in clinical practice, and that their results were valid only for their simulated signals used. In another paper, Emmanuel Roy, Pierre Abraham, Silvio Montresor, and Jean-Louis Saumet investigated the performance of different time-frequency distributions (TFD) to detect high-intensity transient signals and concluded that smoothed-pseudo-wigner-ville distribution (SPWVD) provided better results than Choi-williams distribution (CWD) and cone-kernel distribution (CKD) [15]. However, the SPWVD, the CWD and the CKD was implemented using FFT. The limitations of such FFT based methods are well known: conflict between time and frequency resolution.

K. Kisman was able to use the FFT to obtain good gas bubble detection rates with Doppler probes implanted directly adjacent to the vein of interest, thereby minimizing the presence of artifacts in the signal [16]. While this work showed that automatic detection of gas bubble was possible, the highly idealized experiment involved invasive procedures and the processing of a signal with virtually no artifacts,

neither of which is applicable to my case.

H. Markus, M. Cullinane, and G. Reid used the conventional FFT in an online program to detect emboli from trans-cranial Doppler measures [17]. This program was shown to perform about as well as a panel of human experts [18]. However, this signal has very low background noise, which makes the detection of embolic signal very easy.

2.1.2 Wavelet-based methods

The wavelet transform is being increasingly applied, in the fields ranging from communications to medicine, to analyze signals with transient or nonstationary components. Nonstationary means that the frequency content of the signal could change over time and the onset of changes in the signal cannot be predicted in advance. Gas bubble signals, which are transient like and of very short duration, fit the definition of nonstationary signals.

Nizamettin Aydin, Soundrie Padayachee and Hugh S. Markus described the embolic signals by the use of continuous wavelet transform (CWT) [19]. The CWT is the ideal method for the detection of constant-velocity (and therefore, constant frequency) embolic signals. However, it is observed that many embolic signals exhibit varying frequency content. In [20], Brian S. Krongold, Akbar M. Sayeed, Mark A. Moehring, James A. Ritcey, Merrill P. Spencer and Douglas L. Jones used time-scale-chirp (Chirp-CWT) detector to detect micro-emboli in the flowing blood

with Doppler ultrasound signal. The CWT (time-scale) was computed utilizing the chirp-z transform and fast convolution [21]. The time-scale-chirp detector used the same CWT for nine different chirp rates, and the generalized likelihood-ratio test (GLRT) search was done over this parameter space.

Nizamettin Aydin, Farokh Marvasti and Hugh S. Markus used the discrete wavelet transform (DWT) to analyze the transcranial Doppler audio signals [22]. These signals were decomposed into a number of frequency bands using DWT. From the experimental result, it was found that almost all gas bubble signals are represented at the first four scales. One drawback of using DWT to the representation of gas bubble signal is the reduced frequency resolution at lower scales, in which gas bubble signal are found mostly. Unfortunately, the DWT produces the good resolution in the low frequency and the poor resolution in the high frequency. This conflicting property prevents the exact representation of Doppler ultrasound signals both in high frequency and low frequency band. In this research, very short samples of gas bubble signals, Doppler speckles and artifacts were used. Each sample contained one feature in isolation – an artifact, Doppler speckle, or an embolic signal. Their algorithm was able to correctly classify the vast majority of 300 such samples. However, artifacts contaminated gas bubble signals and Doppler speckles dominated gas bubble signals were not taken into account in their research. Occasionally, the signals used in the research could be found in the human

body.

Ping-Wing Lui, Brent C. B. Chan, Francis H. Y. Chan, Paul W. F. Poon, Hsin Wang, and F. K. Lam carried out an experiment on seven dogs for the detection of venous emboli using DWT [23]. The experiment is performed in two phases. 10 minutes gap was taken between the phases. In the first phase, a series of emboli (0.01, 0.02, 0.05, 0.07, 0.1, 0.15, 0.2, 0.3, 0.4, and 0.8mL) are injected into the external jugular vein through the catheter. Emboli are injected by using a micro-syringe (Hamilton, Reno, NV) at intervals of 2-5 minutes. Then in the second phase, a series of larger emboli (0.8, 1.6, 2.4, 4.8, and 9.6 mL) was injected at various controlled rates of 0.011-0.128 $mL \cdot kg^{-1} \cdot min^{-1}$ over 5 minutes by using a precalibrated syringe pump (Model PSK-01; Nikkiso Co. Ltd., Tokyo, Japan). The emboli used in this experiment are very large in size with respect to the emboli found in human body. The method used in the detection of emboli was found useful. However, the algorithm is not properly applicable to the small emboli detection in the human body due to the difference in nature between the small emboli and the larger emboli. On the other hand, the signals taken from dogs were analyzed by DWT. Signal power was calculated from the wavelet coefficients and emboli were detected by the use of predefined threshold on the signal power. It is very difficult to set a standard threshold for different kinds of signals.

2.1.3 EMD-based methods

M. A. Chappell and S. J. Payne proposed an automated approach [24] for the detection of gas bubbles using empirical mode decomposition (EMD). In this research, gas bubble monitoring was performed into the pulmonary artery. This location is preferred because it is very close to the body surface. Another point is that it allows observing the rate of gas bubble production in the entire venous system, as all the returning blood from the body must pass through the pulmonary artery. The signal taken from pulmonary artery was decomposed into a series of nonstationary and band-limited components called intrinsic mode functions (IMFs), whose character is not predefined. Theoretically, the IMFs represent the effects of different physical processes in the Doppler ultrasound signal. In [25], Hamilton and Tompkins proposed a robust approach for the detection of peaks or QRS complex, primarily to improve the detection accuracy of QRS complexes in ECG signals. Chappell and Payne modified Hamilton and Tompkins original algorithm and employed the modified algorithm to the IMFs for the detection of systolic phase. The signals used to detect systolic phase are collected in a different arrangement to the signals used to detect QRS complexes. This allows raising a question to the detection of systolic phase from Doppler ultrasound signals using the algorithm based on QRS complex detection algorithm. In fact, QRS complex detection algorithm or modification of that algorithm could be applicable to the low graded

Doppler ultrasound signals for the detection of systolic phase. It is illustrated in Fig. 2.1 and Fig. 2.2. Low graded or grade-0 signal is shown in Fig. 2.1 and the systolic phase detection from that signal is shown in Fig. 2.2. However, for high graded Doppler ultrasound signals more advanced algorithm is required. In [24], the gas bubble detection algorithm relies upon the determination of peak systole in the cardiac cycles. A search region is defined between consecutive peaks of systoles within which it is suspected that features of gas bubble could be found. Detection of any false peak systole in the cardiac cycle could alter the consequences.

In this research, a huge number of thresholds were determined for the purpose of gas bubble detection. In fact, it is difficult to set a threshold that excludes all the false events, such as those caused by blood cell movement, opening or closing of valves and other noise related events without excluding smaller bubbles. In that case this method is found to be limited.

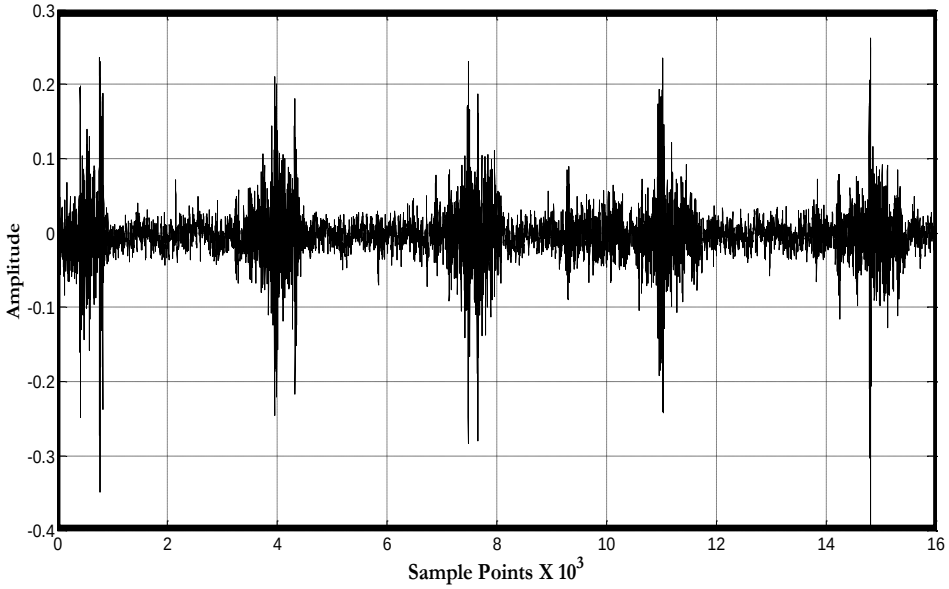

Fig. 2.1: Low graded Doppler ultrasound signal

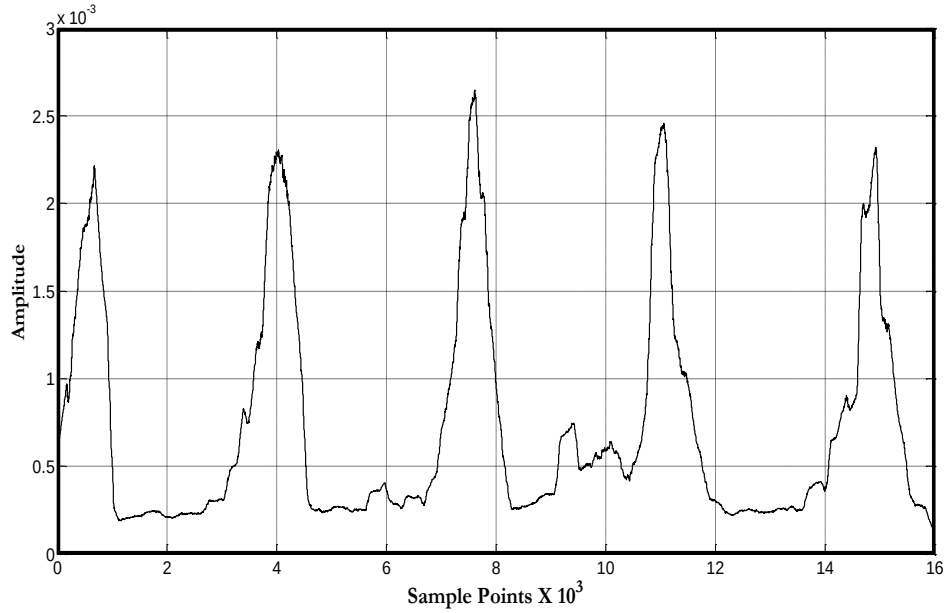

Fig. 2.2: Systolic phase detection from the above low graded Doppler ultrasound signal

2.1.4 Parametric model based methods

Jean-Marc Girault, Denis Kouame, Abdeldjalil Ouahabi and Frederic Patat presented an embolic detection methods based on parametric signal processing approaches [26]. This parametric model is a time-variant autoregressive (AR) model. The basic idea of this research is to compare the Doppler embolic signal to its autoregressive model. The Doppler signals containing one gas bubble or at best two gas bubbles were used in their experiment. However, high graded Doppler gas bubble signals were not used or could not be modeled in the study.

2.1.5 LPC-based methods

Takayoshi Nakai, Masahiro Watanabe and Hisayoshi Suzuki discovered some features of the gas bubble signals in the time domain and in the frequency domain, and developed a gas bubble detection method based on linear predictive signal processing [27]. The signals taken from pulmonary artery are processed in this research. In the signals, systolic phase is predicted by using the linear predictive analysis and it is removed. As the general property of the linear predictive analysis, the prediction is accurate for the periodic signal, resulting in smaller errors and smaller residual signal. By applying the linear prediction for a relatively long time, the regular component in the Doppler signal, which is due to the heartbeat, could be predicted for low graded Doppler ultrasound signals. Consequently the algorithm could be effective for the low graded

signal. By contrast, the prediction error or residual signal increases for the nonstationary signals. The signals containing gas bubbles are considered as nonstationary signals due to its very short duration and transient like nature. Therefore, it is very difficult to predict the systolic phase from the mixture of gas bubble signals and systolic phase signals, more specifically for high graded signals, since the gas bubble signal occurs irregularly and suddenly in the high graded signals. For high graded signals more efficient algorithm should be employed for the purpose of systolic phase detection. The bloodstream during the systolic phase is either a turbulent flow or close to the turbulence. Then, the sound of the systolic phase or peak systole could have a complicated spectrum similar to that of the gas bubble signal. It is observed that many gas bubble signals exists in the systolic phase for grades I, II and III. In that case it is very difficult to discriminate the signals representing gas bubbles from the systolic phase signals. From such a viewpoint, the systolic phase should not be removed from the signal.

Once the systolic phase is removed, a two-step decision making procedure is applied to the signal. A sub-segment representing the gas bubble is extracted from the signal based on the amplitude and the number of zero-crossings. Only these two parameters are inadequate for the detection of gas bubble signals. Moreover, the spectral peaks are determined by the linear prediction from the extracted sub-segment and the

approximate center of the peak frequency is determined by visual inspection, to be defined as the central frequency of the gas bubble signal, which is very much subjective, not quantitative.

2.2 Research objectives and contributions

Disease due to gas bubble is a significant risk to the caisson workers. A major clinical challenge, particularly in an emergency room, is to quickly and correctly diagnose patients with gas bubble and then send them on to therapy. Many research works are carried out to the detection of gas bubble. However, a major problem with clinical implementation of the systems is the lack of a reliable and efficient algorithm of gas bubble detection. In this study, an efficient algorithm for the detection of gas bubble from Doppler ultrasound signal is proposed on the basis of a two-phase processing. In the first phase, systolic phase is detected. In the second phase, gas bubble is detected. The systolic phase detection plays an important role in the field of gas bubble detection. By detecting the systolic phase, search regions are defined within which it is suspected that features of gas bubble could be found. Due to nonstationary nature of the Doppler ultrasound signal, it is decomposed into IMFs by using EMD. The IF, the instantaneous amplitude and the instantaneous phase of each real valued IMF are calculated by applying DHT. HS is generated to represent these IF, instantaneous amplitude and time. Then an improved visualization to the HS is proposed. In this improved HS, one

parabolic shape appears in each of the cardiac cycles within which systolic phase and gas bubble could be found. Systolic phase is isolated from this HS through the reconstruction of the signal. However, further processing is required to the detection of gas bubble. Therefore, in the second phase another algorithm is proposed. This HS based representation requires only the number of frequency bins as the input parameter and does not include cross-spectral term. Hence, it performs better as demonstrated by the experimental results. This algorithm is more effective for the detection of systolic phase. The main advantage of this approach is that it is valid for low graded signal as well as high graded signal.

In the second phase, time-varying mean frequency is derived from the instantaneous amplitude and the IF. This time-varying mean frequency exhibits some smooth and increasing trends. It is most likely that these trends are responsible for the gas bubble signal or other similar events. An interesting algorithm is employed to extract the trends or segments. These trends are belonging to the gas bubble signal or other similar events. Considering physical properties of the gas bubble signal, some features or parameters are derived from the segments in time-varying mean frequency domain. To ensure more accuracy, other parameters are derived in time domain based on IMFs. All these parameters are used and a decision is made to the detection of gas bubble on the basis of fuzzy logic rule. In most of the research works, either frequency

domain or time domain signal processing is carried out. In this research, to achieve more accuracy time-varying mean frequency domain and time domain signal processing is performed.

It is envisioned here that this research should be implemented in a true on-line system which can operate in real time. It is believed that this research could help to study the clinical significance of gas bubble in the bloodstream, in more quantitative terms while also significantly impacting the treatment modalities and thus tremendously improving the patient care.

CHAPTER 3

Development of an algorithm for systolic phase detection

3.1 Systolic phase detection

Systolic phase detection is challenging if the signal contains decompression-induced gas bubbles. The sequence of mechanical and electrical events that repeats with every heartbeat is called the cardiac cycle. A single cycle of cardiac activity can be divided into two basic phases – systolic and diastolic phase. It is observed that decompression-induced gas bubble passes through the pulmonary artery during the systolic phase. The formation of gas bubbles in the bloodstream are due to rapid changes in environmental pressure that could happen while carrying out construction work under water (caisson), flying or scuba diving. The bubbles remaining in the body could block many vessels or compress nerves and result in various functional disorders, including strokes and even death. Such disorders are called decompression syndromes (DCS) or caisson disease. The gas bubble monitoring relies upon the detection of individual systolic phase.

The first aim of this study is to detect systolic phase from Doppler ultrasound signal. Detecting systolic phase from Doppler ultrasound signal is challenging if the signal belongs to high grade in terms of gas bubble detection rate. Spencer and Johanson in [28] defined Doppler ultrasound signal grades according to the rate of

bubble detection. In another study by Chappell and Payne in [29], where only two types of Doppler ultrasound signals are considered to detect systolic phase using EMD. However, the correspondence between the signals used in [29] and the signal grades defined by Spencer in [28] is not clear. Using EMD systolic phase can be detected from the electrocardiogram by the detection of QRS complex, is published in [30]. It can also be detected from other types of signals, e.g. cardiac output and arterial pressure signals are discussed in [38][39]. The detection result from different signals could be different, since there is a time delay in the different signal types. This is due to the fact that the cardiac output and arterial pressure describe the vaso-mechanical properties of the heart while electrocardiogram and Doppler ultrasound describe the electrical activity and mechanical properties respectively.

In this chapter, an efficient algorithm is proposed for the purpose of systolic phase detection from the high graded Doppler ultrasound signal. In the literature, very often systolic phases are detected in time domain analysis. In the case of low graded signals, a simple time domain algorithm can be used to detect systolic phase. However, it cannot provide a description of how systolic phase energy evolves over time. Whereas, in the case of high graded signals, the analysis is not simple and identification of the systolic phase shape and the time when it occurs are difficult. Such an analysis is proposed in the current study using time-frequency-energy representation of the

Doppler ultrasound signal. In this study, the signal shown in Fig. 3.1 is decomposed into a finite number and band-limited IMFs using EMD, then the instantaneous frequency (IF) is derived for each component. All the IFs are scaled between 0 and 0.5 and multiplied by a weighting factor and the bin spacing of the HS is selected. The overall HS is defined as the weighted sum of the instantaneous amplitudes of all the IMFs at the frequency bin. Therefore a new time-frequency-energy representation is determined from the IMFs using HS. This new representation offers a clue to the detection of systolic phase. The properly detection of the systolic phase is the most important task to detect gas bubbles associated DCS.

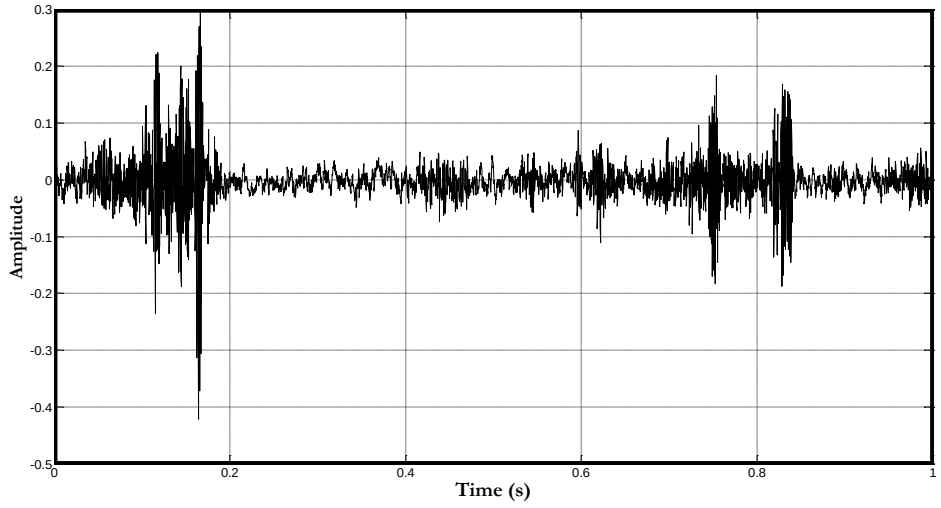

Fig. 3.1: Doppler ultrasound signal

3.2 Method of systolic phase detection

The Hilbert spectrum (HS) is a relatively new joint time-frequency representation introduced in [31]. Two phases are required to generate the HS. In the first phase, EMD is employed, which is an adaptive decomposition method [32]. Then DHT is employed in the second phase. HS is generated by the combination of EMD and DHT. This is an adaptive analysis method, especially useful for nonlinear and non-stationary signal analysis.

At a normal heart rate (80 beats per minute), a period is considered to be 0.8 seconds. Atrial systole, ventricular systole, and diastole take approximately 0.1 second, 0.3 seconds and 0.4 seconds respectively. One period Doppler signal must contain 4000 samples (N) if the sampling frequency is 5000 Hz and heart rate is 80 beats per minute. Since heart rate of the Doppler signal during the recording time could not be at such rate, one period of the obtained signal could be longer or shorter than 4000 samples. Therefore, the sample duration considered in the study is one second and it is thought that within that limit there should be at best two systolic phases.

3.2.1 EMD Basics

Empirical mode decomposition (EMD) focuses on the level of local oscillations and decomposes the signal into a finite set of AM-FM oscillating components which are bases of the decomposition. The bases into which the signal is decomposed are obtained

from the signal itself, and they are defined in the time domain. The principle of the EMD technique is to decompose a signal $s(t)$ into a sum of the band-limited functions $\alpha_m(t)$ or bases called intrinsic mode functions (IMFs). Each IMF satisfies two basic conditions: (i) in the whole data set, the number of extrema and the number of zero crossings must be the same or differ at most by one, (ii) at any point, the mean value of the envelope defined by the local maxima and the envelope defined by the local minima is zero. The first condition is similar to the narrow-band requirement for a stationary Gaussian process and the second condition is a local requirement induced from the global one, and is necessary to ensure that the instantaneous frequency will not have redundant fluctuations as induced by asymmetric waveforms.

3.2.2 Univariate EMD (uEMD)

The univariate EMD (uEMD) is used to decompose the univariate signal into a finite set of IMFs. There exist many approaches of computing EMD [33]. The following algorithm is employed here to decompose signal $s(t)$ into a set of IMF components. The process of extracting an IMF from a signal is called "the sifting process".

1. Set $u_1(t) = s(t)$, where $s(t)$ and $u_1(t)$ represents the original signal. $u_1(t)$ is used as a temporary variable.
2. Find the extrema (both maxima and minima) of $u_1(t)$.
3. Generate the upper and lower envelopes $h(t)$ and $l(t)$ respectively by

connecting the local maxima and local minima separately with cubic spline interpolation (e.g., linear, spline, piece-wise spline). In this paper the linear method is chosen.

4. Calculate the local mean as : $\mu_1(t) = [h(t) + l(t)]/2$.

5. IMF should have zero local mean; subtract $\mu_1(t)$ from the original signal as: $u_1(t) = u_1(t) - \mu_1(t)$.

6. Decide whether $u_1(t)$ is an IMF or not by checking the two basic conditions as described above.

7. Repeat steps 2 to 6 until an IMF $u_1(t)$ is found.

Once the first IMF is derived, we define $\alpha_1(t) = u_1(t)$, which is the smallest temporal scale in $\mathrm{s}(t)$. In order to find out the rest of the IMF components, the residue $\varepsilon_1(t)$ of the data is generated by subtracting $\alpha_1(t)$ from the signal $\mathrm{s}(t)$ as $s(t) - \alpha_1(t) = \varepsilon_1(t)$. The sifting process will be continued until the final residue is a constant, a monotonic function, or a function with only one maxima and one minima from which no more IMF can be derived.

The subsequent basis functions and the residues are as $\varepsilon_1(t) - \alpha_2(t) = \varepsilon_2(t), \dots, \varepsilon_{M-1}(t) - \alpha_M(t) = \varepsilon_M(t)$, where $\varepsilon_M(t)$ is the final residue. At the end of the decomposition, the signal $\mathrm{s}(t)$ is represented as: $s(t) = \sum_m \alpha_m(t) + \varepsilon_M(t)$, where $\varepsilon_M(t)$ is the final residue which can be either the mean trend or a constant, and

functions $\alpha_m(t)$ are not guaranteed to be mutually orthogonal, but often are close to orthogonal, and all have zero means [31]. The EMD (individual IMF) of Doppler signal is illustrated in Fig. 3.2. 6 IMFs out of 13 IMFs are shown in Fig. 3.2. More specifically, the first component has the smallest time scale which corresponds to the fastest time variation of the data. As the decomposition process proceeds, the time scale increases, and hence, the mean frequency of the mode decreases [33]. Since the decomposition is based on the local characteristic time scale of the data to yield adaptive basis, it is applicable to nonlinear and non-stationary data in general and in particular.

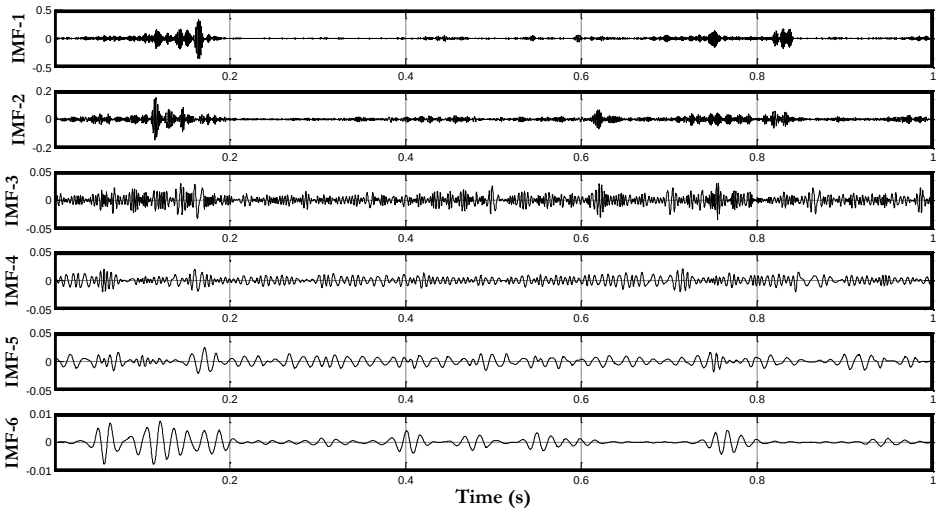

Fig. 3.2: Extraction of six IMFs through the decomposition of the signal

3.2.3 Discrete Hilbert transform

The notion of frequency and energy for each IMF is obtained by employing the concept of analytic signals. The discrete Hilbert transform (DHT) is used to compute the analytic signal for an IMF. The analytic signal $Z_m(t)$ corresponding to the m_{th} IMF $\alpha_m(t)$ is defined as

$$Z_m(\mathrm{t}) = \alpha_m(t) + jH_D[\alpha_m(t)] = \gamma_m(t)e^{j\theta_m(t)}, \tag{3.1}$$

where $\gamma_m(t)$ and $\theta_m(t)$ are instantaneous amplitude and phase respectively of the m_{th} IMF. The discrete Hilbert transform $H_D[.]$ is defined as

$$H_D[\alpha_m(t)] = \frac{1}{\pi}\sum_{\tau=1,\tau\neq t}^{T}\frac{\alpha_m(\tau)}{t-\tau} \ . \tag{3.2}$$

The analytic signal is advantageous in determining the instantaneous quantities such as energy, phase and frequency. The IF of m_{th} IMF is then given as the derivative of the phase $\theta_m(t)$–calculated at *t* i.e.

$$f_m(t) = \frac{\partial\tilde{\theta}_m(t)}{\partial t}, \tag{3.3}$$

where $\tilde{\theta}_m(t)$ represents the unwrapped version of instantaneous phase $\theta_m(t)$. The derivative in Equation 3.3 is evaluated at discrete instant of time *t*. It should be noted that such derivative introduces the abrupt fluctuations of IF and hence nonlinear smoothing is required. Here, the moving average smoothing filter is used to remove such fluctuations. The filtering scheme improves the effectiveness of computing IF using discrete derivative. The IF of individual IMF shown in Fig. 3.2 is illustrated in Fig.

3.3. The concept of IF is physically meaningful only when applied to mono-component signals. In order to apply the concept of IF to arbitrary signals it is necessary to decompose the signals into a series of mono-component contributions. In the recent approaches [31], EMD technique decomposes a time domain signal into a series of mono-component IMFs. Then the IF derived for each component provides the meaningful physical information.

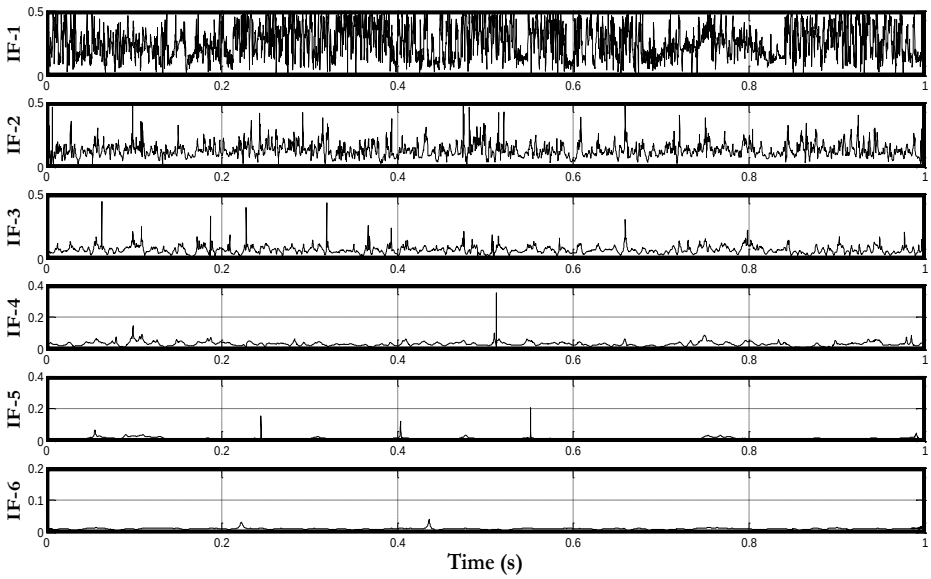

Fig. 3.3: The IFs of the selected (1st to 6th) IMF components

Although the IMFs may have frequency overlaps but at any time instant, the instantaneous frequencies represented by each IMF are different. This phenomenon can be well understood in Fig. 3.3 which shows the instantaneous frequencies of the first 6 IMFs of the Doppler signal shown in Fig. 3.2. Therefore, EMD is an effective decomposition of non-linear and non-stationary signals in terms of their local frequency

characteristics. With such property, each frequency component of the signal is clearly identified and localized in both time and frequency scales yielding spectra at each sampling point.

3.2.4 Hilbert spectrum

Having obtained the IMFs as a result of the sifting process and IFs from each IMF, it is possible to generate the HS, or a three dimensional (3D) plot that represents the distribution of the signal energy as a function of time and frequency. In the figure time, frequency and energy are plotted on the X-coordinate, Y-coordinate and the Z-coordinate respectively. All the IFs are scaled between 0 and 0.5 and multiplied by the equation $\lambda = 0.5/(IF_{max} - IF_{min})$ for simplifying the generation of HS, where IF_{max} and IF_{min} is the maximum and minimum IF calculated from all the IFs. The bin spacing of the HS is 0.5/B, where B is the number of desired frequency bins. The overall HS is defined as the amalgamation of the spectra of each of the IMFs. Hence, each element $H(b,t)$ in the overall HS is defined as the weighted sum of the instantaneous amplitudes of all the IMFs at the b_{th} frequency bin.

$$H(b,t) = \sum_{m=1}^{M} \gamma_m(t)\omega_m^{(b)}(t), \tag{3.4}$$

$$\varphi(b,t) = \sum_{m=1}^{M} \theta_m(t)\omega_m^{(b)}(t), \tag{3.5}$$

where the factor $\omega_m^{(b)}(t)$ is equal to 1 if $\lambda \times f_m(t)$ (normalized instantaneous frequency) lies between two consecutive frequency bins, otherwise it is 0. Normalized instantaneous frequencies found from all the IMFs are not plotted in the cell of HS. Its corresponding instantaneous amplitude is plotted in the cell of HS using Equation 3.4. After computing the elements over the frequency bins, *H* represents the instantaneous signal spectrum in time-frequency (TF) space [34]. Fig. 3.4 illustrates the Hilbert spectrum of the Doppler ultrasound using 256 frequency bins. It is noted that the time resolution of *H* is equal to the sampling rate and the frequency resolution can be chosen up to the Nyquist limit [35]. During the construction of the Hilbert spectrum, the phase matrix $\varphi(b,t)$ representing the phase information corresponding to each time-frequency cell of $H(b,t)$ is saved. In Fig. 3.4, only one color is plotted for all the levels of energy except the zero level. For zero level nothing is plotted. Low frequency components energy are contributing more and high frequency components energy are contributing less in the HS.

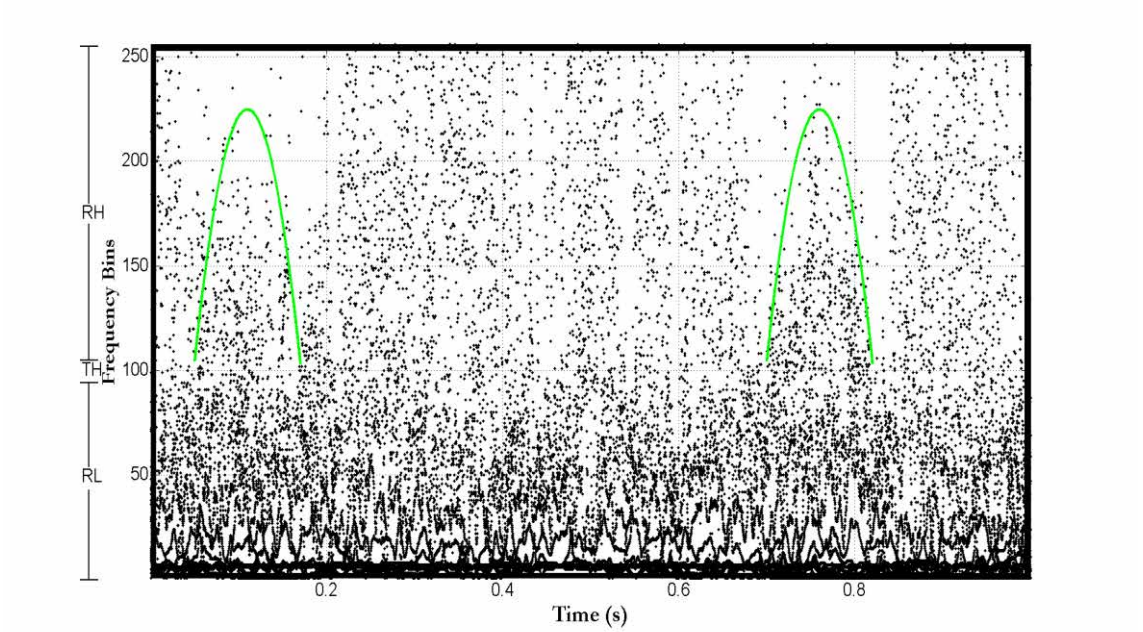

Fig. 3.4: Hilbert spectrum of the Doppler ultrasound signal showing two parabolic shapes

3.2.5 High frequency energy to low frequency energy ratio

Our aim is to observe the synchrony between systolic phases in time domain with energy activities in the HS. With the intention of easing the interpretation of the HS, a threshold (TH) is determined to separate the HS into two regions, the region of low frequency components energy (RL) and the region of high frequency components energy (RH). The choice of the threshold is performed visually from the HS. It is observed that the RL is visually uniform throughout the spectrum. However in RH, two parabolic shapes are found (Fig. 3.4) which corresponds to the approximate location of two systolic phases and gas bubbles in time domain. The systolic phase could be detected within any location of the parabolic shape. This is due to the variation in timing

between systolic phase sound and pulmonary valve opening sound. However, another algorithm is required to detect gas bubble in the parabolic shape. The region between two parabolic shapes is also visually uniform. In RL, the low frequency components energy is summed up over the frequency bins at every time instant as $\mathrm{L(t)} = \sum_{b=1}^{TH} HS(t)$. Similarly in RH, $\mathrm{H(t)} = \sum_{b=TH+1}^{B} HS(t)$. Ratio between L(t) and H(t) is defined as RA(t)=H(t)/L(t) and plotted in Fig. 3.5.

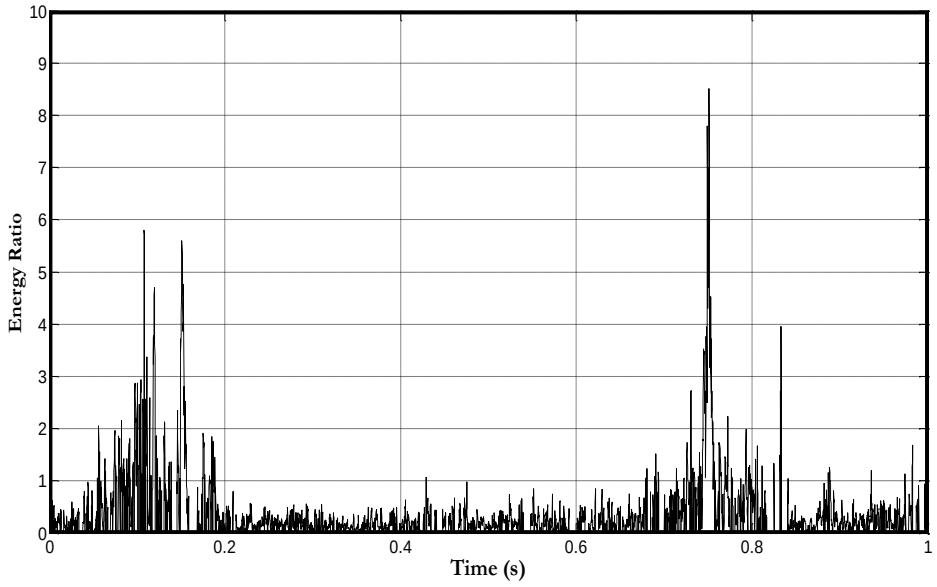

Fig. 3.5: Ratio between high frequency energy and low frequency energy

3.2.6 Signal reconstruction

Systolic phase detection from RA(t) is obtained by signal reconstruction. Since RA(t) is derived from HS, distribution of RA(t) and HS is similar. Regarding the distribution of RA(t) and HS the main difference between those two terms is that one is represented by the energy ratio at every instant of time, whereas the other is represented by energy over

all the frequency bins at every instant of time. The time domain signal representing systolic phase is calculated by element wise multiplication of *RA(t)* and the cosine of the phase vector $\varphi(b,t)$ as

$$sp(t) = RA(t) \cdot \cos[\varphi(b,t)], \tag{3.6}$$

where the signal containing systolic phase is designated by $\mathrm{sp}(t)$. In order to obtain a unique maximum for each systolic phase, $\mathrm{sp}(t)$ is filtered through the low pass Butterworth filter of order ten. Having detected the systolic phase from the first block (one second signal) of the Doppler ultrasound, the same detection method is repeated for all other blocks of the signal. The order of the detected systolic phases is maintained and all the blocks are concatenated. The result shows that the detected systolic phases are well represented and localized in the figure. In Fig. 3.6 two systolic phases are detected which appear to be correct as detected by medical specialist.

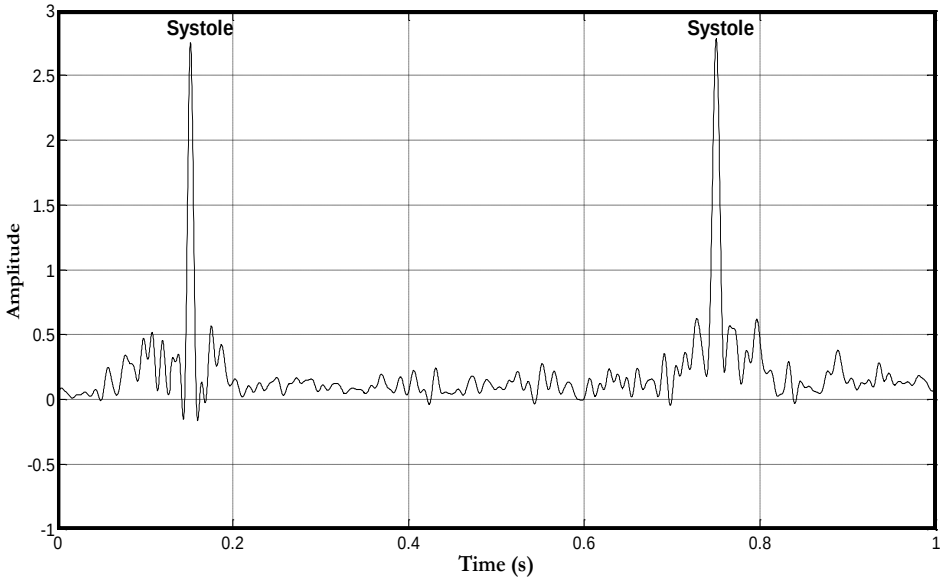

Fig. 3.6: Two systolic phase in two cardiac cycles

3.3 Results and discussions

In the experiment, four levels (grades) of signal are considered to demonstrate the performance of the proposed method. In case of low graded signals very simple algorithm is required to detect systolic phase. On the other hand very efficient algorithm is required to detect systolic phase from high graded signals. Such algorithm could be used in the first phase to the detection of gas bubble.

The study in [29], there are two parts. In the first part systolic phases are detected from Doppler ultrasound but the performance of this detection algorithm is not discussed. Which makes it difficult to compare the method with our proposed method. Some algorithms are proposed in [36][39][37] to detect systolic phase from ECG,

cardiac output and arterial pressure signals but variation is found between the times of occurrence of successive systolic phase in the different signal types. Moreover, these signals are derived in an entirely different manner to the signal used here. Hence, again it is difficult to compare this to the method presented here.

Therefore, the two most essential parameters used here for describing the overall performance of the systolic phase detection are: sensitivity SE and positive predictivity PP. The sensitivity reports the percentage of true systoles that are correctly detected. The positive predictivity reports the percentage of detected systoles which are in reality true systoles. The sensitivity and positive predictivity of the detection algorithms are computed by

$$\mathrm{SE}(\%) = \frac{TP}{TP+FN} * 100, \tag{3.7}$$

$$\mathrm{PP}(\%) = \frac{TP}{TP+FP} * 100, \tag{3.8}$$

where TP is the number of true positives, FN the number of false negatives, and FP the number of false positives. The systolic phase detection result is illustrated in Table 3.1. Over 97 percent of the systolic phases are detected from grade 0 and grade 1 signal. In case of grade 2 signals, over 97 percent of the systolic phases are detected. However, for grade 3, the detection performance of our proposed algorithm is not as efficient as that for grade 2. All the grades of the signal are divided into two groups. In the first group first three grades are considered and the remaining grades are considered in another

group. It should be noted that these results may be influenced by the choice of the TH values.

Table 3.1: Results of evaluation of the proposed algorithm

Grade	Systolic phase	TP	FN	FP	SE(%)	PP(%)
0	20	20	0	0	100	100
0	20	20	1	0	95	100
1	20	20	0	0	100	100
1	20	19	1	1	95	95
2	20	20	0	0	100	100
2	20	19	1	1	95	95
3	20	14	3	2	83	88
3	20	13	3	3	82	82
4	20	0	0	0	0	0
4	20	0	0	0	0	0

CHAPTER 4

Signal segmentation

4.1 Time-varying mean frequency

The time-varying mean frequency is expressed in terms of the time waveform [40]. The results obtained from the time-varying mean frequency could give a strong motivation for time-frequency analysis. Considering first,

$$\begin{aligned} \mathrm{W}s(t) &= \mathrm{W}\gamma(t)e^{j\theta(t)} \\ &= \frac{1}{j}\frac{d}{dt}\gamma(t)e^{j\theta(t)} \\ &= \left(\theta'(t) - j\frac{\gamma'(t)}{\gamma(t)}\right)s(t). \end{aligned} \tag{4.1}$$

For convenience, the frequency operator can be defined as,

$$\mathrm{W} = \frac{1}{j}\frac{d}{dt} \ .$$

Therefore, the mean frequency is

$$\begin{aligned} \langle\omega\rangle &= \int \omega|S(\omega)|^2 d\omega \\ &= \int s^*(t)\frac{1}{j}\frac{d}{dt}s(t)dt \\ &= \int \left(\theta'(t) - j\frac{\gamma'(t)}{\gamma(t)}\right)\gamma^2(t)dt \ . \end{aligned} \tag{4.2}$$

In the case of mean frequency it can be proved that

$$\begin{aligned} \langle\omega\rangle &= \int \omega|S(\omega)|^2 d\omega \\ &= \frac{1}{2\pi}\iiint \omega\, s^*(t)s(t')e^{j(t-t')\omega}d\omega dt'dt \end{aligned}$$

$$= \frac{1}{2\pi j}\iiint s^*(t)s(t')\frac{\partial}{\partial t}e^{j(t-t')\omega}d\omega dt'dt$$

$$= \frac{1}{j}\iint s^*(t)\frac{\partial}{\partial t}\delta(t-t')s(t')dt'dt$$

$$= \int s^*(t)\frac{1}{j}\frac{d}{dt}s(t)dt \quad . \tag{4.3}$$

In Equation 4.2, the second term is zero. This can be seen in two ways. First, since that term is purely imaginary it must be zero for $\langle\omega\rangle$ to be real. Alternatively, we note that the integrand of the second term is a perfect differential that integrates to zero. Hence

$$\langle\omega\rangle = \int \theta'(t)\,|s(t)|^2dt$$

$$= \int \theta'(t)\,|\gamma(t)|^2dt \quad . \tag{4.4}$$

This is an interesting and important result because it says that the mean frequency could be obtained by integrating something with the density over all time. This something must be the instantaneous value of the quantity for which we are calculating the average. In this case the something is the derivative of the phase, which could be appropriately called the frequency at each time or the instantaneous frequency $f(t)$,

$$f(t) = \theta'(t) \quad . \tag{4.5}$$

In the case of IMF, Equation 4.4 can be defined in terms of instantaneous amplitude and instantaneous frequency [41],

$$F_\mu(t) = \sum_{m=1}^{M}\gamma_m^2(t)\,f_m(t), \tag{4.6}$$

where M is the number of IMF and $F_\mu(\mathrm{t})$ is the time-varying mean frequency. The time-varying mean frequency is determined by using Equation 4.6 and given in Fig. 4.1.

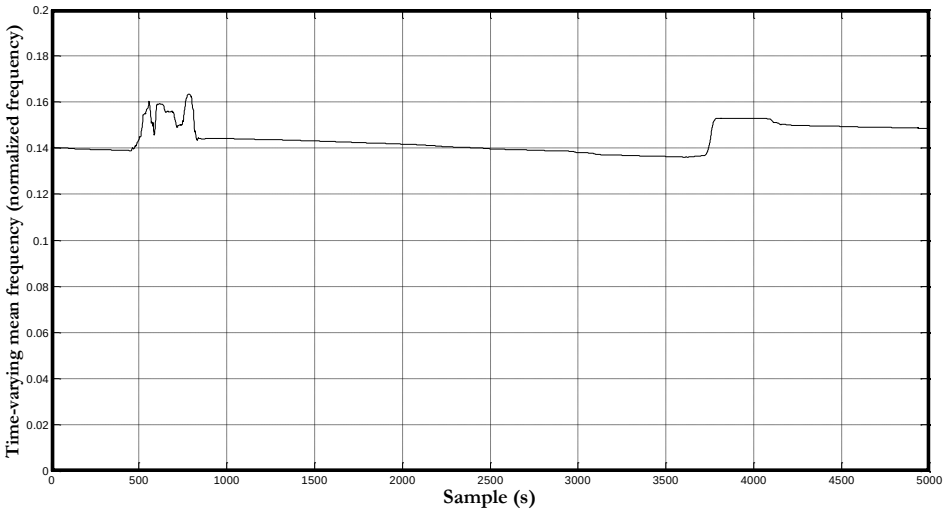

Fig. 4.1: Time-varying mean frequency

4.2 Signal segmentation algorithm

Usually, specific part of a signal belonging to a specific event is determined by various algorithms of signal processing using signal characteristics of its waveform such as signal frequency, amplitude, phase, time duration, time-varying mean frequency, morphology and etc. It is found that the choice of the algorithm depends on the characteristics of the signal. It is observed that gas bubble signal appear as very smooth increasing trend in the time-varying mean frequency. An algorithm is applied to the time-varying mean frequency to extract the segments belonging to the very smooth increasing trend. These segments could be either gas bubble or other similar events. It is proved in the next chapter that these segments are representing either gas bubble or not on the basis of gas bubble features. At first the time-varying mean frequency is segmented into small sub-segments. Considering the gas bubble signal length, small

sub-segments length is determined. It is observed that three or more sub-segments are required to make a segment which could be gas bubble signal. The detection of the segment representing gas bubble could be difficult when the length of the sub-segment is selected inappropriately. A large sub-segment could have some characteristics of gas bubble signal and some characteristics of other signal. On the other hand, a small sub-segment not representing gas bubble signal could be found between two other small sub-segments representing gas bubble signal. In this thesis, the length of the sub-segment is determined empirically. Each sub-segment is taken into account to calculate the average slope S_{μ}. Three parallel lines are drawn in Fig. 4.2. First sub-segment between first and second line is shown and second sub-segment between second and third line is shown. Similarly the remaining part of the signal is segmented and the following algorithm is applied. Close snapshot of the sub-segments in Fig. 4.2 is taken and illustrated in Fig. 4.3.

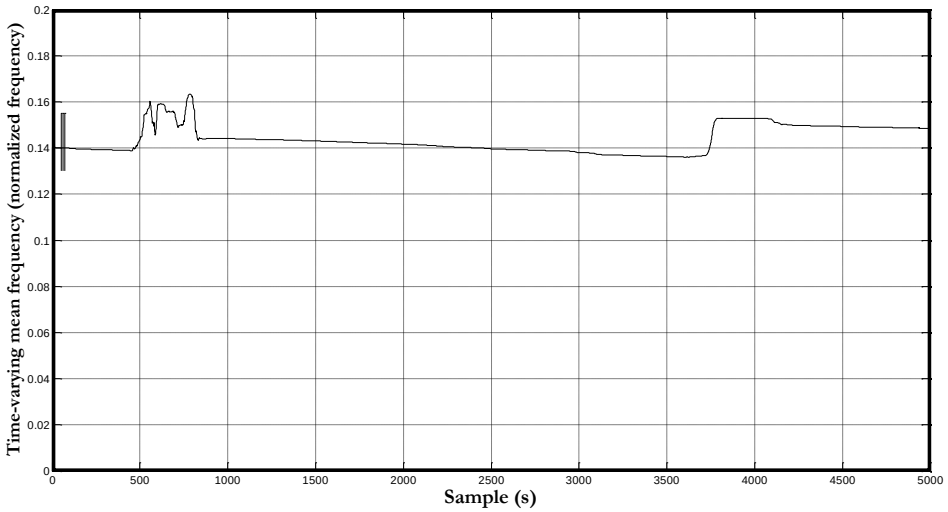

Fig. 4.2: Sub-segments in time-varying mean frequency

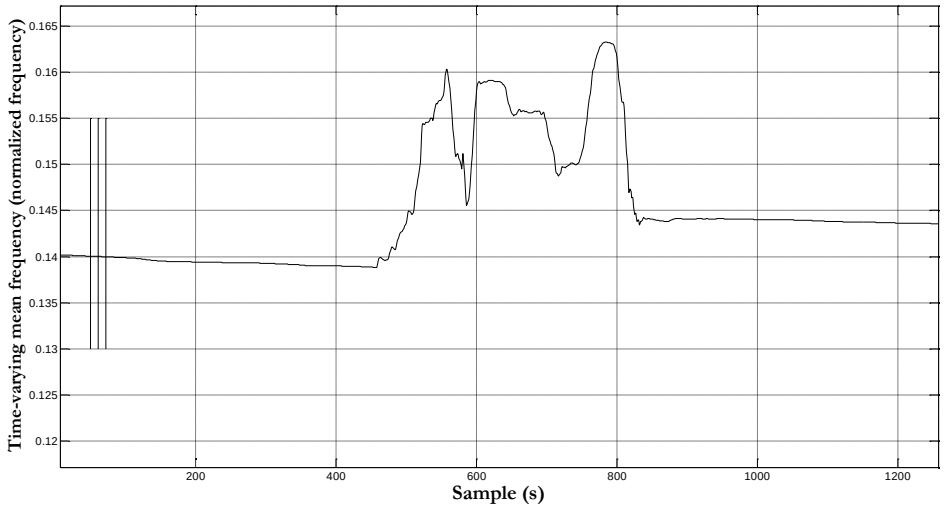

Fig. 4.3: Close snapshot of sub-segments in time-varying mean frequency

4.2.1 Ascending slope tracing algorithm

Since the signal below the threshold is not concerned, the signal is filtered before segmenting the signal. The time-varying mean frequency obtained in the previous section is divided into a number of sub-segments. In this research, a simple but interesting algorithm is introduced to process these sub-segments based on signal

characteristic such as amplitude, average slope, and deflection width. The consecutive sub-segments having those characteristics are merged to generate a segment which could be gas bubble.

Each sub-segment is numbered and processed serially using the ascending slope tracing algorithm. An array having length equal to the number of sub-segments is used during the processing of the sub-segments. Initially, all the array elements are zero. The average slope of the sub-segment is calculated by dividing the accumulated time-varying mean frequency difference between neighboring N+ 1 samples by N using Equation 4.7.

$$S_{\mu} = |\sum_{i=n-N+1}^{n} (x[i] - x[i-1])/N| \ , \tag{4.7}$$

where N+1 is the number of samples of each sub-segment. Then the following algorithm is applied to that sub-segment. If the sub-segment can satisfy the algorithm, its corresponding number is inserted into the array. Once all the sub-segments are processed, the consecutive sub-segment numbers are counted. Three or more consecutive sub-segments are merged and considered a new segment for further processing. The numbering scheme is illustrated in Fig. 4.4. In Fig. 4.4, sub-segments 2, 3 and 4 are merged and considered a new segment. Similarly, sub-segments 8, 9, 10 and 11 are merged and considered as a new segment.

0	2	3	4	0	0	0	8	9	10	11	0	0	0	0	0

Fig. 4.4: An array for processing the sub-segments

The steps of the algorithm are as follows:

Step 1: A sub-segment is taken and average slope $S_{\mu 1}$ is calculated. Once all the sub-segments are processed, go to step 7.

Step 2: If $S_{\mu 1}$ is greater than zero, it is saved. Otherwise go to step 1.

Step 3: Next sub-segment is taken and average slope $S_{\mu 2}$ is calculated. Once all the sub-segments are processed, go to step 7.

Step 4: If $S_{\mu 2}$ is greater than zero, it is saved. Otherwise, go to step 1.

Step 5: The following two conditions are tested

- $S_{\mu 1}$ is greater than 75% of $S_{\mu 2}$.
- $S_{\mu 2}$ is greater than 75% of $S_{\mu 1}$.

If condition 1 or condition 2 is satisfied, numbers of both sub-segments are placed directly into its corresponding position in the output array.

Step 6: Set $S_{\mu 1}$=$S_{\mu 2}$ and go to step 3.

Step 7: If at least three or more than three consecutive sub-segments are found into the array, all the sub-segments are merged and considered it as a segment. This segment is considered as a candidate to be gas bubble. In the next chapter it is proved that either

this segment in time-varying mean frequency domain is representing gas bubble or not.

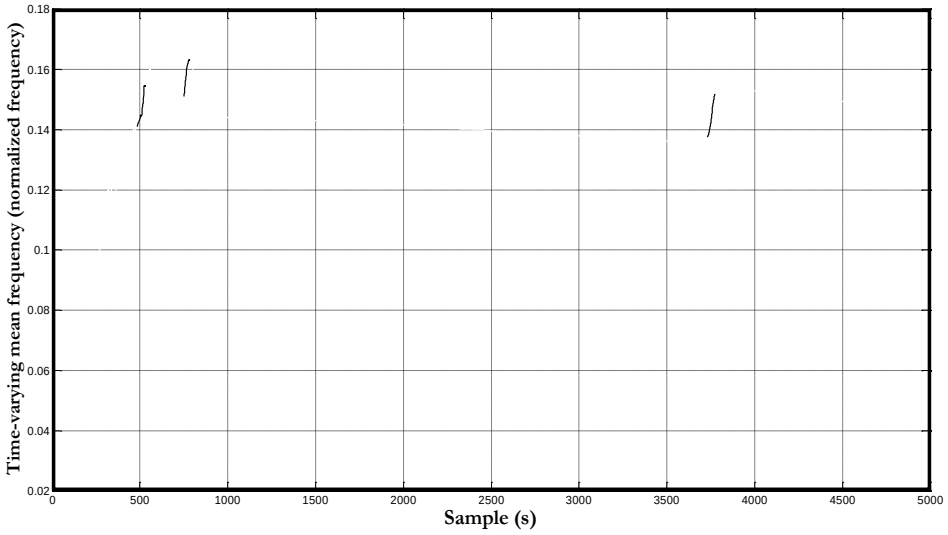

Fig. 4.5: Three segments in time-varying mean frequency

The above algorithm extracts three segments, as shown in Fig. 4.5. Larger version of these segments is shown in Fig. 4.6, 4.7 and 4.8 respectively. Sometimes, other parts of the signal not belonging to gas bubble are obtained using this algorithm. In Fig. 4.6, such a segment is obtained. It is most likely that this segment could belong to the cardiac valve opening sound.

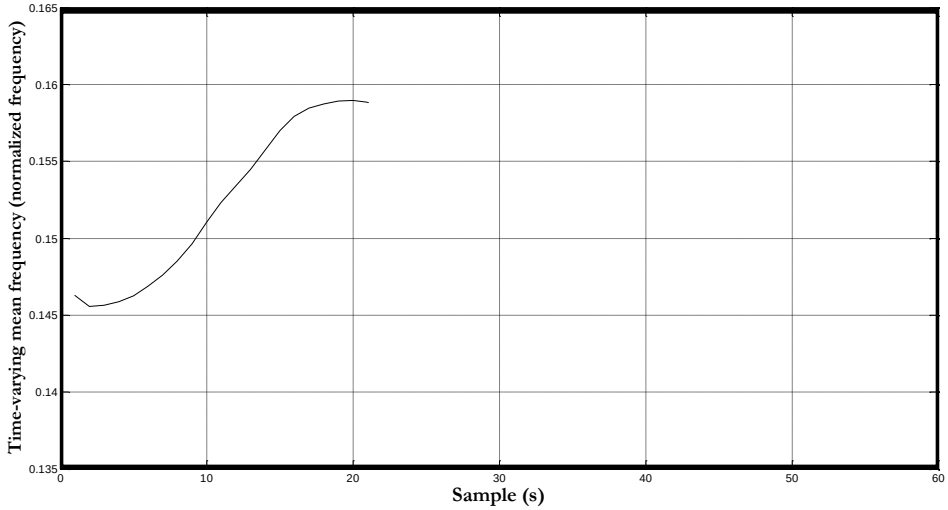

Fig. 4.6: Larger version of first segment out of three segments

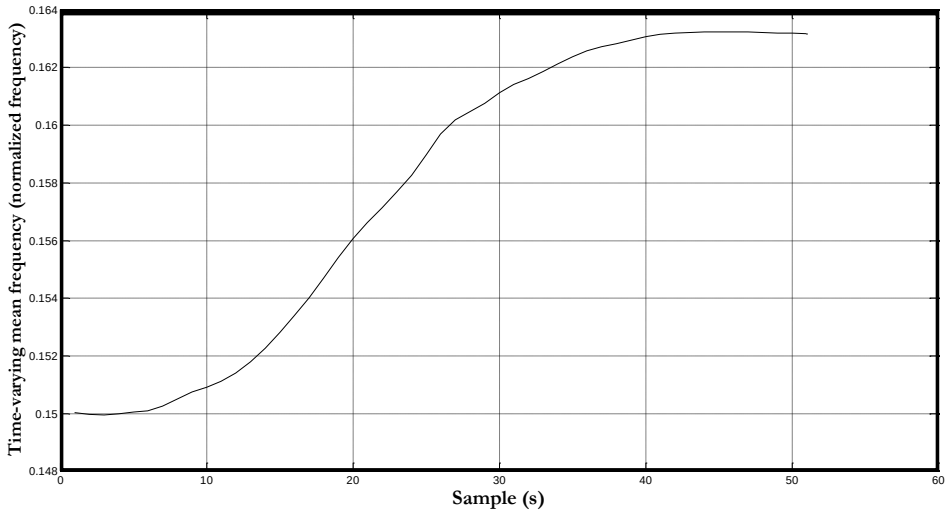

Fig. 4.7: Larger version of second segment out of three segments

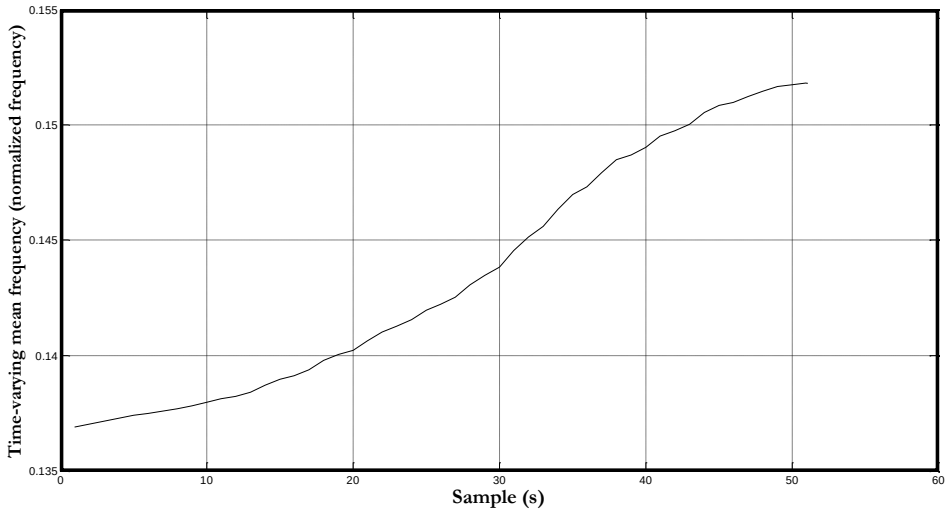

Fig. 4.8: Larger version of third segment out of three segments

CHAPTER 5

Defining the parameters

5.1 Finding the parameters from segments

All the segments found in the last chapter are used in this chapter to find out some parameters. Some parameters are determined from the segment of time-varying mean frequency domain and some parameters are determined from the corresponding segment, but in IMF-based time domain. The segment in time-varying mean frequency domain which could belong to the gas bubble signal or other events is decided on the basis of calculated parameters in that domain. Similarly, the same segment in IMF-based time domain which could belong to the gas bubble signal or other events is decided based on the parameters in that domain. In fact, validation is performed in two domains for the same segment. In the following sections, at first the parameters in time-varying mean frequency domain are discussed, then the parameters in IMF-based time domain are discussed.

5.2 Parameters in time-varying mean frequency domain

Many segments could be found in the time-varying mean frequency domain. The segments are very much similar. However, some parameters could discriminate the gas bubble segments from other segments. It is found that the following parameters are very useful to the detection of gas bubble segment.

5.2.1 Spreading in frequency (F_S)

Many gas bubble signals exhibit varying frequency content. Gas bubble signal is described as "frequency focused" as well as "short duration" high intensity transients. It is believed that spreading in frequency could play a vital role to discriminate between gas bubble signals and other related events. The segments representing either gas bubble signal or other events such as valve motion, blood cell movement or systolic phase in time-varying mean frequency domain are taken into account to determine the spreading in frequency. It is defined as,

$$F_S = \sum \left(F_I(t) - F_\mu(t)\right)^2 S_B^2(t), \tag{5.1}$$

where S_B is obtained by summing or integrating sections of the IMFs. Residue is not considered. Sections of the IMFs corresponding to the segment of time-varying mean frequency are extracted. A segment in time-varying mean frequency domain and its corresponding sections in IMFs are shown in Fig. 5.1 and 5.2 respectively. Then, S_B is defined as,

$$S_B = \sum_{m=1}^{M} a_m(t), \tag{5.2}$$

where the section of IMF is represented by a and M is the number of IMF. Similarly, sections of the IFs corresponding to the same segment are taken and summed up. Sections of each IF are shown in Fig. 5.3. Then, F_I is defined as,

$$F_I = \sum_{m=1}^{M} \omega_m(t), \tag{5.3}$$

where the section of IF is denoted by ω and M is the number of IF. In Equation 5.1, time-varying mean frequency is designated by F_{μ}.

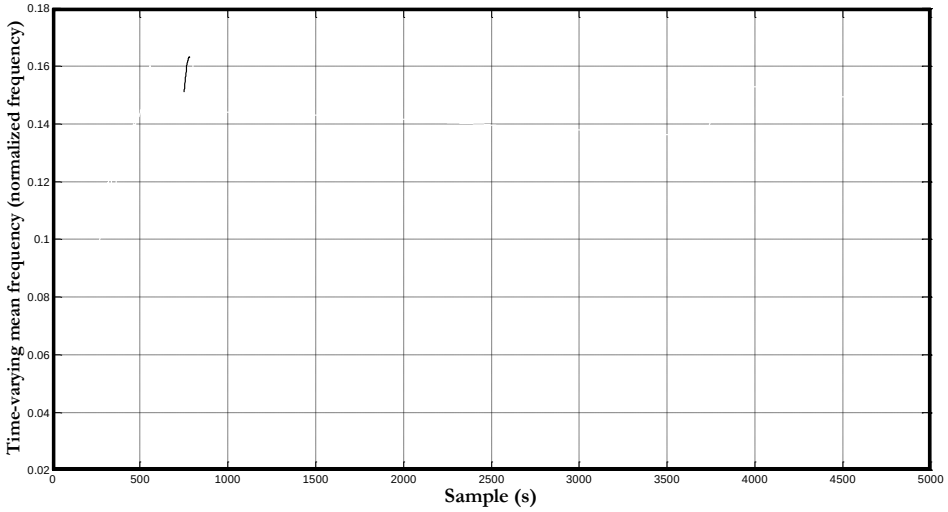

Fig. 5.1: Segment in time-varying mean frequency domain

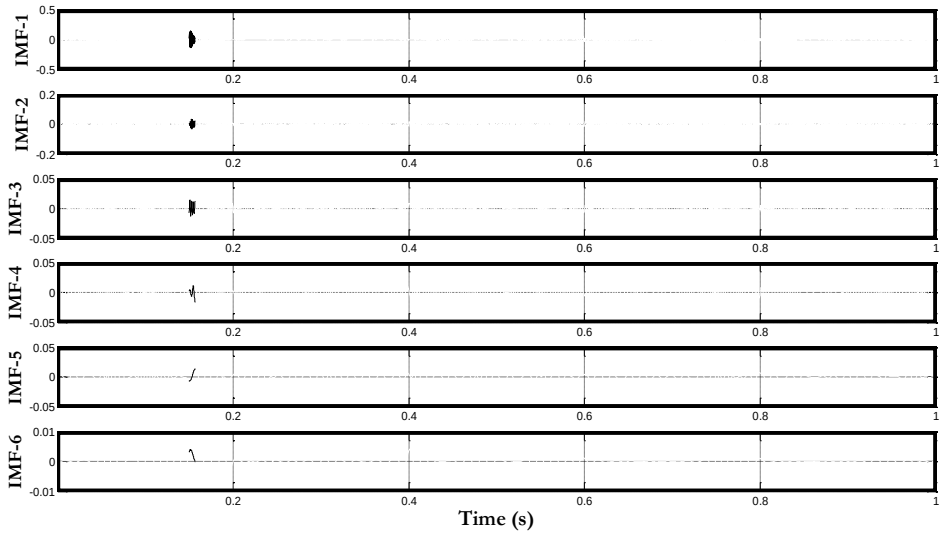

Fig. 5.2: Segment corresponding section in IMFs

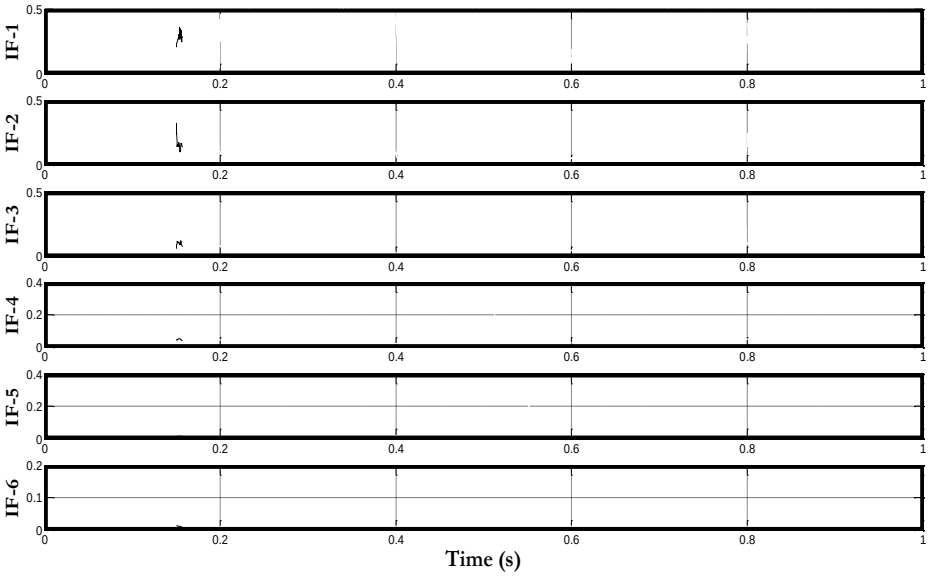

Fig. 5.3: Segment corresponding section in IFs

5.2.2 Ratio of the gas bubble signal to the background signal (R_{BB})

Ratio of the gas bubble signal to the background signal is determined to show that how strong a gas bubble signal is with respect to the background signal. In [42], M. A. Moehring and J. R. Keppler introduced this ratio. The R_{BB} is the major character which is used to distinguish gas bubble signal from the normal blood signals [43]. Also, the R_{BB} could be applied to evaluate the gas bubble diameter [44]. The R_{BB} is defined as follows,

$$R_{BB} = \frac{P_S}{P_B} \ , \tag{5.4}$$

where P_S is the power at time-varying mean frequency with maximum intensity. It is determined from the segment, which is considered as candidates for gas bubbles. P_B is the average power of the background signal in time-varying mean frequency domain.

All the segments found by applying the ascending slope tracing algorithm are removed from the time-varying mean frequency. The remaining sections, as shown in Fig. 5.4 are taken into account to calculate the P_B. The remaining sections are taken to perform addition and divided by the time interval. It is defined as,

$$P_B = \frac{1}{t_2 - t_1} \sum_{t=t_1}^{t_2} F_\mu^2(t) \quad . \tag{5.5}$$

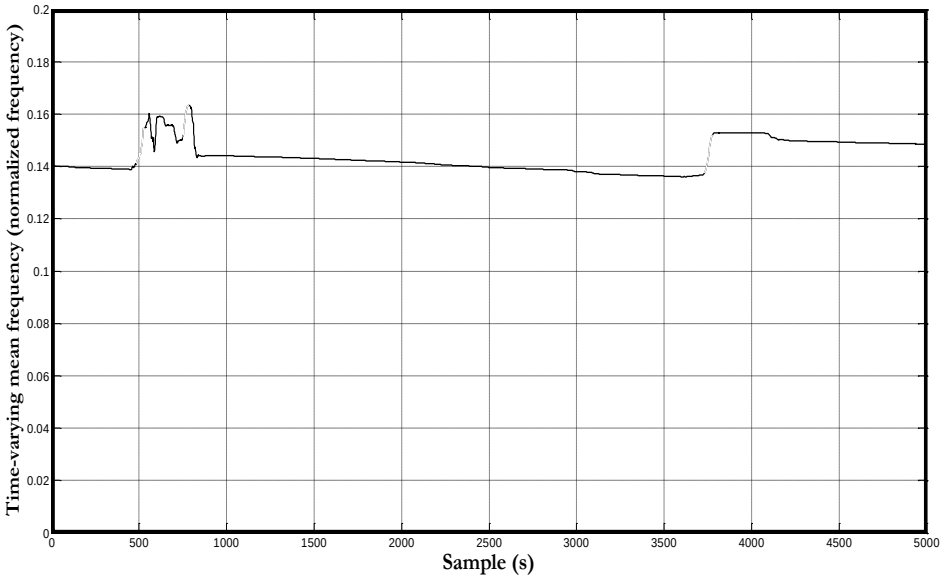

Fig. 5.4: The remaining sections after removing the segments

5.2.3 Ratio of the gas bubble signal's total power to the background signal (R_{TB})

When the gas bubble signal passes through the Doppler sample volume, there is band-limited and high-intensity transient in the backscattered ultrasonic power, which is usually larger than the level of the background blood signal [45][46]. Ratio of the gas bubble signal's total power to the background signal is determined to realize the amount

of power a gas bubble signal has with respect to the background signal. This property provides an important basis for the gas bubble signal detection. However low R_{TB} could make the differentiation between gas bubble signal and other similar events unreliable. The R_{TB} is defined as,

$$R_{TB} = \frac{P_T}{P_B} \ , \tag{5.6}$$

where P_T is the gas bubble signal's total power. It is determined from the segment extracted from the time-varying mean frequency. The P_T is defined as,

$$P_T = \sum_{t=t_a}^{t_b} F_\mu^2(t) \ . \tag{5.7}$$

P_B is the average power of the background signal, already defined in Equation 5.3.

5.2.4 Rising rate of the gas bubble signal (R_B)

Time-varying mean frequency is derived from the IF and instantaneous amplitude of the IMFs. It is very difficult to find out any clue from the IF and the instantaneous amplitude for the detection of gas bubble signal. However, a smooth increasing trend is figured out in the time-varying mean frequency domain. It is found that all of the increasing trends are not representing gas bubble signal. Some of them are representing gas bubble signals. Therefore, the rising rate representing gas bubble signal is determined. The R_B is defined as,

$$R_B = \frac{P_X - P_M}{t_b - t_a} \ , \tag{5.8}$$

where P_X is the maximum power obtained from the segment of time-varying mean

frequency. Similarly, P_M is the minimum power obtained from the same segment. $t_b - t_a$ is the time duration of the segment.

5.3 Parameters in IMF-based time domain

Some parameters similar to those of time-varying mean frequency domain are defined in this section. However, the following parameters are defined in IMF-based time domain. The parameters in time-varying mean frequency domain are plying a vital role to the detection of gas bubble signal. In addition to this, to achieve more accuracy, the parameters in IMF-based time domain are defined. In fact, the original signal is not used in determining the parameters. Instead of the original signal, some selected IMFs of the original signal are used.

5.3.1 Spreading in time (T_S)

Section of each IMF corresponding to the segment of time-varying mean frequency is extracted to define the spreading in time. The reason for defining the section's time spreading is that it could correspond to the gas bubble signal. In addition to this, it could provide a gross characterization of the signal density and it could provide an indication of where the density is concentrated. Many measures can be used to ascertain whether the density is concentrated around the average, the most common being the spreading in time T_S, given by,

$$T_S = \sum \left(T_I(t) - T_\mu(t)\right)^2 S_D^2(t), \tag{5.9}$$

where T_μ is the average time of the segment. S_D is obtained from the section of each IMF. The section of each IMF corresponding to the segment in time-varying mean frequency is summed up and designated as S_D. If S_D^2 is considered as a signal density in time, the average time can be defined in the usual way.

$$T_\mu = \sum_{t=t_a}^{t_b} T_I(t) \cdot S_D^2(t), \tag{5.10}$$

where t_a is the time of the segment's first sample and t_b is the time of the segment's last sample. In a small interval of time, the segment takes $S_D^2(t) \cdot T_I(t)$ amount of energy to produce the segment at that time.

5.3.2 Ratio of the gas bubble signal to the background signal (T_{BB})

Ratio of the gas bubble signal to the background signal is determined for time-varying mean frequency domain in the previous section. In this section, this parameter is determined in IMF-based time domain. Because of different acoustic properties between the gas bubble signal and the red blood cell signal, the high-intensity transient in the temporal waveform of the Doppler ultrasound signal provides a simple way to detect the gas bubble signal [47]. The T_{BB} is given as follows,

$$T_{BB} = \frac{E_S}{E_B}\ , \tag{5.11}$$

where E_S is the segment's maximum energy at time t. This segment does not belong to the time-varying mean frequency domain. It belongs to the combination of IMFs or

IMF-based time domain signal. The segment found in time-varying mean frequency domain is taken into consideration, and then its corresponding section in combined IMFs is extracted. E_S is obtained from this section of IMFs. E_B is the average energy of the background signal in IMF-based time domain. It is determined from the IMFs. The E_B is defined as,

$$E_B = \frac{1}{t_2 - t_1} \sum_{t=t_1}^{t_2} \frac{1}{M} \sum_{m=1}^{M} a_m(t), \tag{5.12}$$

where the IMF is represented by a and M is the number of IMF. Taking into account the segments of time-varying mean frequency domain, its corresponding sections in IMFs are removed and the remaining sections are integrated and divided by M using the Equation 5.12. Then it is divided by the time interval $t_2 - t_1$, time duration of the whole signal to obtain E_B. Diastolic phase, some parts of systolic phase, noises and valve motions could contribute to the E_B.

5.3.3 Ratio of the gas bubble signal's total energy to the background signal (T_{TB})

The segment is taken from the IMFs to calculate the T_{TB}, as in section 5.2.2. The T_{TB} is defined as,

$$T_{TB} = \frac{E_T}{E_B} \ , \tag{5.13}$$

where E_T is the segment's total energy in IMF-based time domain. Since S_D^2 is the energy per unit time it could be appropriately called the energy density or instantaneous power. If S_D^2 is the energy per unit time, then the total energy is obtained by summing or integrating over the time interval $t_b - t_a$, where $t_b - t_a$ is the time interval of the segment. The E_T is given as,

$$E_T = \sum_{t=t_a}^{t_b} S_D^2(t). \tag{5.14}$$

E_B is the average energy of the background signal in IMF-based time domain. It is defined in Equation 5.12.

5.3.4 Rising rate of the gas bubble signal (T_B)

In time-varying mean frequency domain, the rising trend representing gas bubble signal is very clear. In IMF-based time domain signal it is not very clear. However, it is useful to discriminate gas bubble signal from diastolic phase. The T_B is defined as,

$$T_B = \frac{E_X - E_M}{t_b - t_a} \quad , \tag{5.15}$$

where E_X is the maximum energy obtained from the segment in IMF-based time domain. Similarly, E_M is the minimum energy obtained from the same segment. $t_b - t_a$ is the time duration of the segment.

CHAPTER 6

Development of an algorithm for gas bubble detection

6.1 Gas bubble detection

Gas bubble is detected on the basis of two sets of parameters; one set contains F_S, R_{BB}, R_{TB}, and R_B; and another set contains T_S, T_{BB}, T_{TB}, and T_B. All these parameters are defined in the previous chapter. Each parameter is belonging to the different range of values. It is very natural since each parameter carrying different meaning. Most of the times a segment having all the valid values for all the parameters is considered as a gas bubble signal. In that case, gas bubble detection is not very difficult. However, sometimes one segment provides some valid values for some parameters which are belonging to the gas bubble signal and some invalid values for the remaining parameters which are not belonging to the gas bubble signal. In that case, taking into account all the parameters for the detection of gas bubble signal is very much challenging. In fact, one single parameter or several parameters cannot provide reliable result for the gas bubble detection. Taking crisp decision on the basis of combination of the parameters is not very much effective in the clinical diagnosis. The fuzzy logic rule based approach, which provides non-crisp decision, is more reasonable in the clinical diagnosis. Using the fuzzy sets theory, the automated gas bubble detection approach which combines all the parameters are proposed in this chapter. Moreover, the fuzzy logic rule based

approach is more suitable for the clinical diagnosis and makes it possible to integrate the automated detection and the expert experience together.

6.2 Membership function

The fuzzy sets theory is proposed by Zadeh in 1965 [48]. Many classes of objects do not have precisely defined membership in the real world, e.g. in the clinical diagnose. So the transition of an object from membership to non-membership is gradual rather than abrupt. In the fuzzy sets theory, the membership function is introduced to characterize the extent to which a parameter belongs to a certain class. A membership function is proposed in this chapter. Four thresholds are used to construct the membership function. The threshold values which are given in Table 6.2 are determined by statistical evaluation of the parameters. The membership function is illustrated in Fig. 6.1. The output-axis is a number known as the membership value between 0 and 1. This trapezoidal membership function is described by four thresholds and it is given by the following expressions.

$$mf_1 = 0 \qquad \text{For } p \le TD1, \tag{6.1}$$

$$mf_{12} = \frac{p-TD1}{TD2-TD1} \qquad \text{For } TD1 < p \le TD2, \tag{6.2}$$

$$mf_{23} = 1 \qquad \text{For } TD2 < p \le TD3, \tag{6.3}$$

$$mf_{34} = \frac{TD4-p}{TD4-TD3} \qquad \text{For } TD3 < p \le TD4, \tag{6.4}$$

$$mf_4 = 0 \qquad \text{For } p > TD4, \tag{6.5}$$

where membership function and parameter values are denoted by mf and p respectively, TD1 and TD4 locate the "feet" of the trapezoidal function and TD2 and TD3 locate the "shoulder" of the trapezoidal function, as shown in Fig. 6.1. These threshold values are very much dependent on the Doppler ultrasound signal. The interval between TD2 and TD3 is little bit longer. This is due to the variation in values of the parameters.

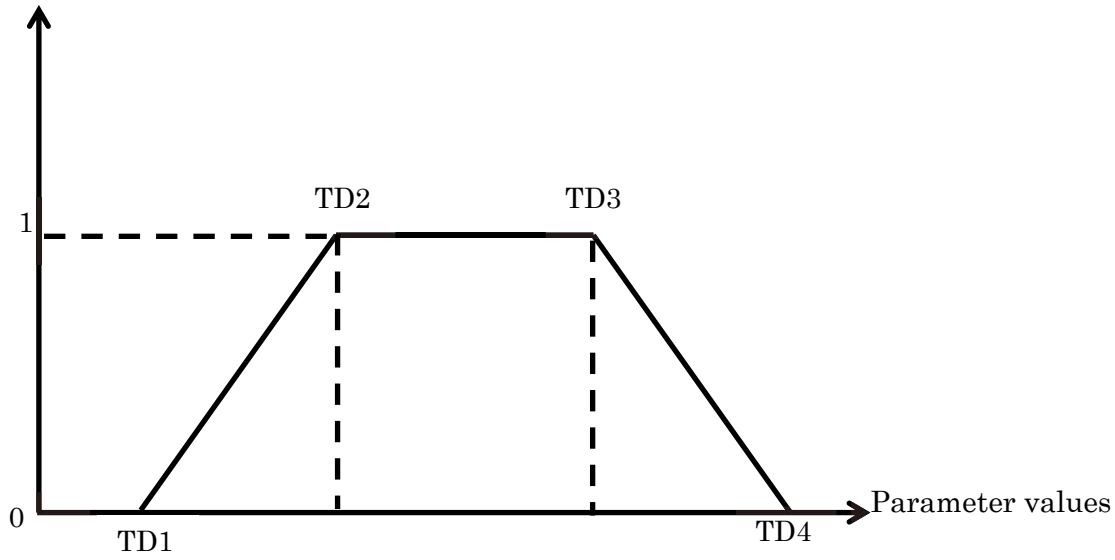

Fig. 6.1: Membership function for the detection of gas bubble signal

6.3 Membership rules and membership values

The membership values for the most parameters are determined according to the membership rules illustrated in Table 6.1, which are derived from the membership function illustrated in Fig. 6.1. Each membership rule consists of a single parameter and their corresponding threshold values. In this way eight membership rules are derived;

four membership rules in time-varying mean frequency domain and four membership rules in IMF-based time domain. It is found that different parameters have four different threshold values. Different threshold values for different parameters are given in Table 6.2. A set of signals containing 50 gas bubble signals are used to determine the thresholds. At first, the parameters defined in the previous chapter are calculated from the 50 gas bubble signals. These 50 gas bubble signals are detected by Doppler ultrasound and gas bubble signal specialists on the basis of visual and hearing inspection. Then, mean and standard deviations for all the parameters are calculated from the gas bubble signals. Considering these mean and standard deviations, threshold values are determined for all the parameters. These threshold values are illustrated in Table 6.2.

Having obtained a segment and its corresponding parameters, membership values are calculated using the Equations 6.1-6.5 and the Table 6.1 for all the parameters. Average of these membership values is determined. The final decision regarding the segment is taken on the basis of average membership values of all the parameters. A segment having an average membership value of 1 is considered as a gas bubble signal or properly “detected” gas bubble signal. On the other hand, a segment having an average membership value between 0 and 1 is considered as a “poorly detected gas bubble signal” or “detected with poor accuracy”. A segment having an average

membership value between 0 and 1 and a threshold value less than TD1 for any of the parameters is considered as a “not detected” gas bubble signal. Similarly, a segment having an average membership value between 0 and 1 and a threshold value greater than TD4 for any of the parameters is considered as a “not detected” gas bubble signal. All the parameters of a segment must have a membership value greater than 0 to be a gas bubble signal. Otherwise, it is not considered as a gas bubble signal. It should be noted that the gas bubble detection results could be influenced by the choice of the threshold values.

Table 6.1: Membership rules for the detection of gas bubble signal

	<=TD1	**>TD1 or <=TD2**	**>TD2 or <=TD3**	**>TD3 or <=TD4**	**> TD4**
F_S	0	mf_{12}	1	mf_{34}	0
R_{BB}	0	mf_{12}	1	mf_{34}	0
R_{TB}	0	mf_{12}	1	mf_{34}	0
R_B	0	mf_{12}	1	mf_{34}	0
T_S	0	mf_{12}	1	mf_{34}	0
T_{BB}	0	mf_{12}	1	mf_{34}	0
T_{TB}	0	mf_{12}	1	mf_{34}	0
T_B	0	mf_{12}	1	mf_{34}	0

Table 6.2: Threshold values of the parameters in the time-varying mean frequency domain and in the IMF-based time domain

	TD1	**TD2**	**TD3**	**TD4**
$\boldsymbol{F_S}$	0.01	0.05	0.25	0.3
$\boldsymbol{R_{BB}}$	0.0005	0.001	0.002	0.0025
$\boldsymbol{R_{TB}}$	0.005	0.01	0.02	0.025
$\boldsymbol{R_B}$	1	1.2	1.8	2
$\boldsymbol{T_S}$	0.02	0.03	0.08	0.09
$\boldsymbol{T_{BB}}$	3	3.5	4	4.5
$\boldsymbol{T_{TB}}$	3	3.5	5.5	6
$\boldsymbol{T_B}$	25	30	40	45

6.4 Results and discussions

The gas bubble signal detection algorithm is applied to the different grades of gas bubble signal. All the grades are discussed in the first chapter. Most of the algorithms for the gas bubble detection provide detection results in the similar way, either gas bubble signal is detected or not. However, a new way is introduced in this research for

showing the gas bubble detection results. A gas bubble signal with an average membership value between 0 and 1 is considered as a “detected with poor accuracy” gas bubble signal. Sometimes, a segment with an average membership value of 1 is obtained. However, it is not gas bubble signal since it is not found in the search region. Therefore, the segment not found in the search region is considered as the “false detection”. Parameters F_S, R_{TB}, T_S, and T_{TB} is playing a vital role to distinguish the gas bubble signal from other events since the whole segment is taken into account to determine the parameters. On the other hand, parameters R_{BB}, R_B, T_{BB} and T_B can provide the similar values for the segments belonging to gas bubble signal as well as other events since the whole segment is not considered in determining the parameters. Gas bubble signal detection results are illustrated in Table 6.3 for different grades of the gas bubble signal.

Table 6.3: Gas bubble signal detection using average membership value

grade	number of gas bubbles	“detected”	“detected with poor accuracy”	“not detected”	“false detection”	data duration
I	50	96%	2%	2%		163 sec
II	50	96%	2%	2%		72 sec
III	50	84%	2%	14%	10%	58 sec

In Fig. 6.2 and 6.3, grade I signal and its corresponding time-varying mean frequency is shown respectively. In the Fig., detected gas bubble signal is marked by the arrow. Similarly in Fig. 6.4, 6.5, 6.6 and 6.7, grade II, grade III signal, time-varying mean frequency and gas bubble signal are shown. In Fig. 6.4 and 6.5, two gas bubble signals are found. In Fig. 6.2, 6.3, 6.6 and 6.7, only one gas bubble is found.

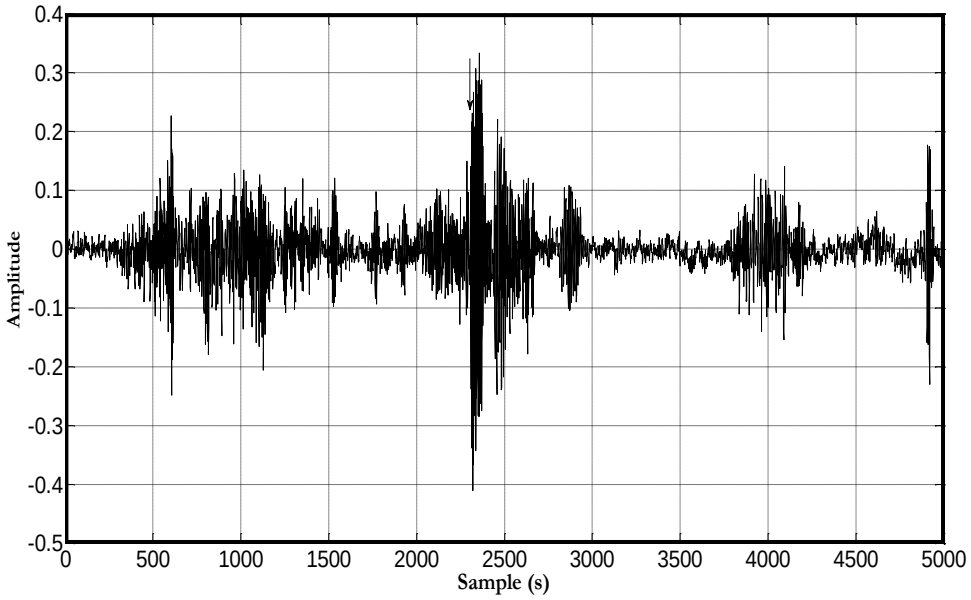

Fig. 6.2: Grade I Doppler ultrasound signal

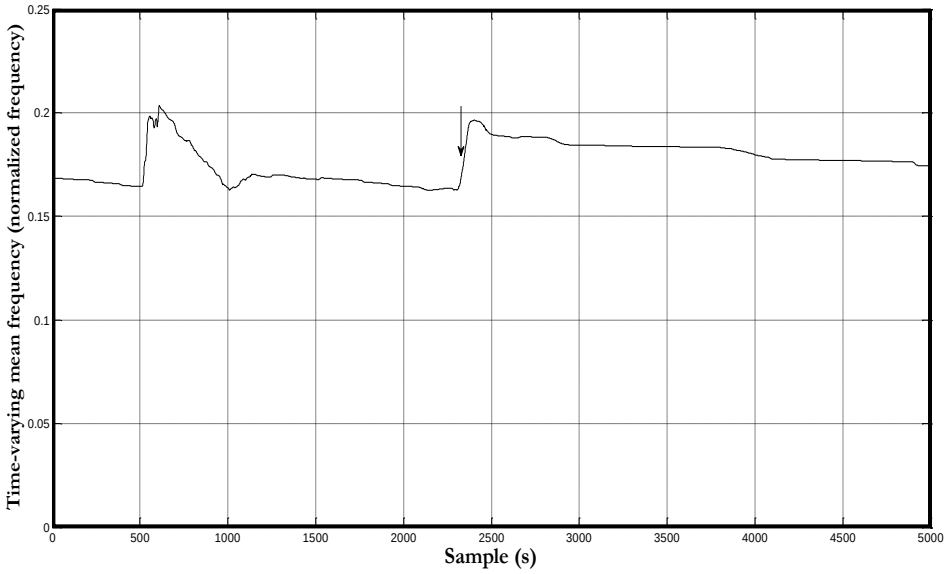

Fig. 6.3: Time-varying mean frequency of Fig. 6.2

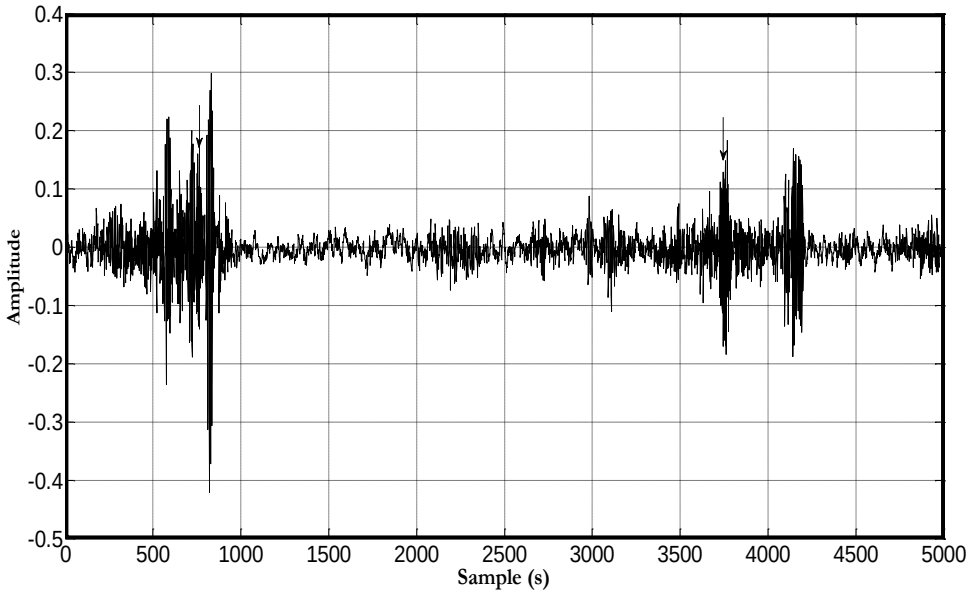

Fig. 6.4: Grade II Doppler ultrasound signal

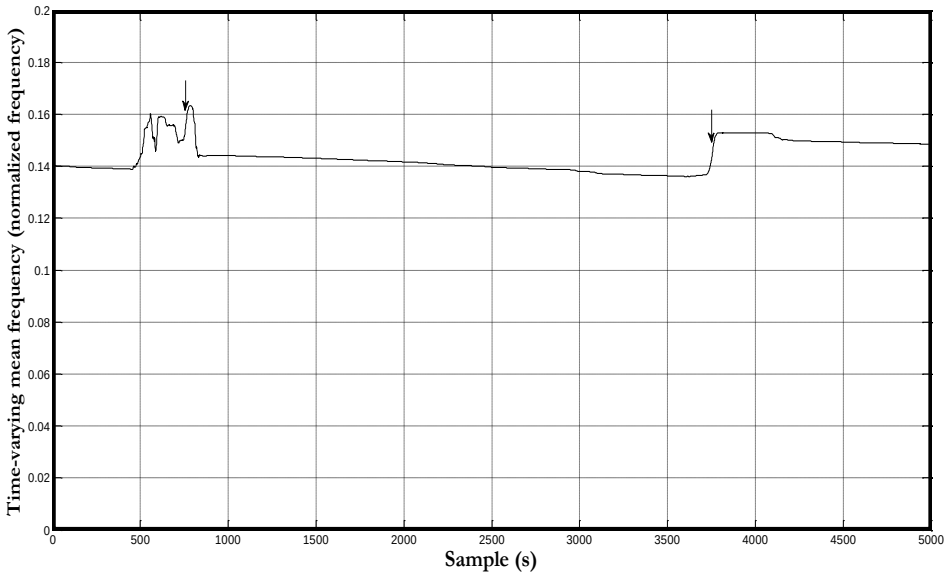

Fig. 6.5: Time-varying mean frequency of Fig. 6.4

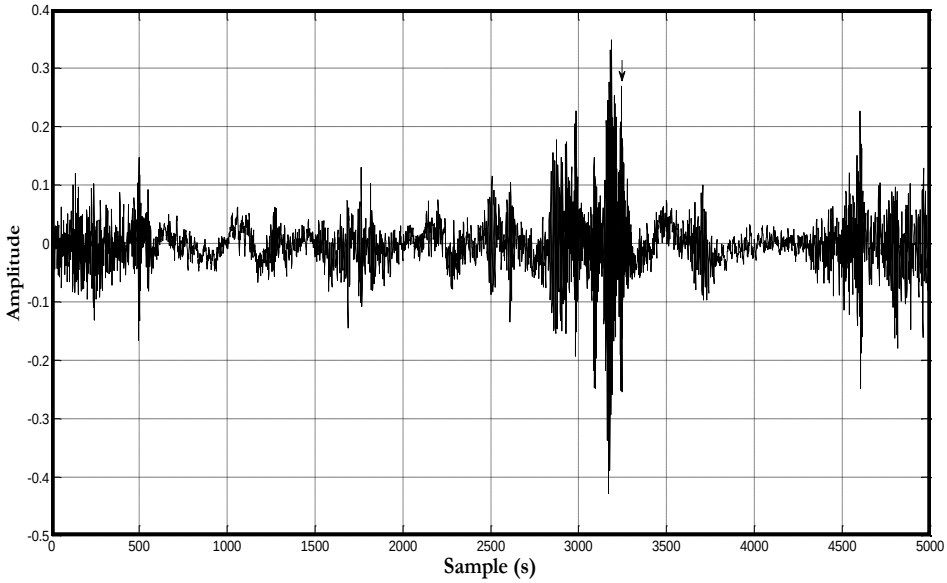

Fig. 6.6: Grade III Doppler ultrasound signal

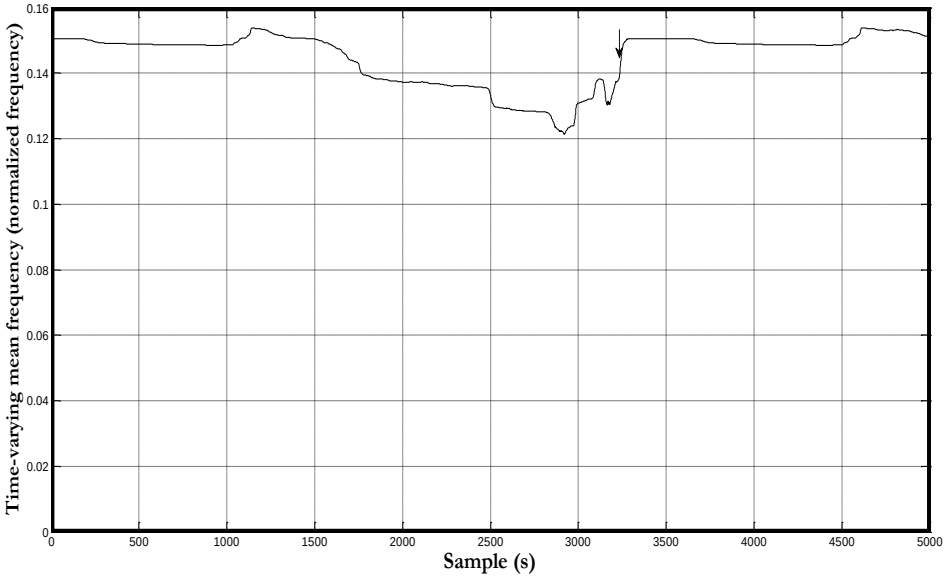

Fig. 6.7: Time-varying mean frequency of Fig. 6.6

In this thesis, an algorithm is addressed for detecting the gas bubbles from Doppler ultrasound signal. We have successfully employed the EMD method to decompose the signal into IMFs. Then DHT is employed to the IMFs to obtain three components; IF, instantaneous amplitude and instantaneous phase. Recently, the EMD and DHT are together used as a potential tool for time-frequency-energy representation (as HS) of time domain signals, especially of nonlinear and nonstationary signals. Therefore HS is generated and a new representation and interpretation of that HS is given. The new representation of HS is focused in this thesis. The new representation of HS can provide the instantaneous spectral information of the Doppler ultrasound signal as well as the overall contribution to the systolic phase and gas bubble signal. The specialty of this new representation of HS is that the time resolution can be as precise as the sampling period and the frequency resolution depends on the choice up to Nyquist limit. Also it does not include cross spectral terms. In the HS, an area with parabolic outline at regular intervals is found within which it is expected that systolic phase and gas bubble signal exists. An algorithm is developed to detect systolic phase in the HS. Systolic phase detection results are illustrated in terms of sensitivity and positive predictivity. In case of grade 0, grade I and grade II signal, over 97 percent of the systolic phases are detected. In case of grade III signal, over 84 percent of the systolic phases are detected. Systolic phase detection could provide the tentative location of gas bubble signal. Hence,

it should be noted that the gas bubble detection is highly dependent on the systolic phase detection. In fact, detecting systolic phase from high graded signal is very much challenging.

In the next step, time-varying mean frequency is derived from IF and instantaneous amplitude. Some smooth increasing trends are found in the time-varying mean frequency. It is observed that these trends or segments could belong to the gas bubble signal or other similar events. An algorithm is developed to extract these segments. Taking into account these segments locations, their corresponding locations in IMFs are extracted and combined. A segment representing gas bubble signal or other similar events are clearly visualized in both domains. Some statistical parameters are determined from the segments of time-varying mean frequency domain and IMF-based time domain. Most of the detection algorithms derive parameters either in frequency domain or in time domain. To achieve more accuracy two sets of parameters in two domains are derived in this thesis; one set of parameters in time-varying mean frequency domain and another set of parameters in IMF-based time domain. Hence, it is playing a significant role to the detection of gas bubble. Some predefined thresholds for each of these parameters are, potentially, be used as input arguments to the fuzzy logic based rules. Each rule is derived strictly for each of the parameters. The membership values found from the fuzzy logic rules are used to calculate an average membership

value for the segment. A segment to be gas bubble must have an average membership value of 1. In addition, it is checked to find the correspondence between this segment location and the search area found in the first phase. A segment having an average membership value between 0 and 1 is termed as “detected with poor accuracy”. Otherwise, the segment does not belong to the gas bubble signal. In case of grade I and grade II signal, over 96 percent of the gas bubble is detected. In case of grade III signal, over 84 percent of the gas bubbles are detected.

CHAPTER 7

Conclusions and future directions

7.1 Conclusions

This thesis has investigated a novel approach to the detection of gas bubble signals from pulsed Doppler ultrasound signal. For this investigation EMD, DHT, new representation of HS, ascending slope tracing algorithm and fuzzy logic rule based method is very adequate. At first, EMD method is employed successfully to decompose the signal. The EMD can be considered as a filter-bank analysis. This filter-bank is an automatic and data adaptive time-variant filtering and especially more suitable in the analysis of nonharmonic signals. DHT is applied to the IMFs to obtain three instantaneous components; instantaneous amplitude, instantaneous phase and IF. Then HS is generated and new representation and interpretation of HS is given by plotting the time-frequency-energy in a different way. It is observed that normally the interpretation of HS is very complex. The complexity of the interpretation of the HS motivated an alternative visualization. This study shows that how a search area or parabolic shape is visualized in the new time-frequency-energy representations. The new representations or new HS found from grade I, II and III Doppler ultrasound signals are very clear. It is observed that gas bubble and systolic phase is found in this new HS. It requires some processing steps to detect systolic phase in the new HS. This new HS illustrates the

empirical relation between time, frequency and energy which is very advantageous to the detection of systolic phase. It is clear that the presence of parabolic shape in time-frequency-energy domain corresponds to the systolic phase in time domain. However, more processing steps are required to the detection of gas bubble signals.

Given instantaneous amplitude and IF, time-varying mean frequency is determined which gives some a clue to the detection of gas bubble signal. An algorithm called ascending slope tracing algorithm is applied to segment the signal. Considering very small sub-segments and merging the sub-segments on the basis of their physical properties is very much challenging. Then the corresponding segments in IMF-based time domain are extracted. The segments in time-varying mean frequency domain and in IMF-based time domain are taken into account to calculate the parameters. A fuzzy logic rule is applied to each of the parameters and membership values are determined. Membership values are very good indicators to show its degree of accuracy in the detection process. In the medical diagnosis, the degree of accuracy is more acceptable than the binary result.

Quantitative results are shown in chapter 3 and chapter 6. In chapter 3, systolic phase detection results are given. A quantitative systolic phase detection efficiency is presented in terms of SE and PP, and obtained very good results for grade I, II and III signals. Similarly gas bubble detection results are given in chapter 6 in terms of average

membership value. As the systolic phase detection, very good detection results for gas bubble signals are achieved for grade I and II signals. For grade III signals, the gas bubble detection results are not as good as the grade I and II. The proposed algorithm is applicable to grade 0, I, II and III signals. In the case of grade 0 signal, there is no gas bubble in the signal. Only systolic phases are found in the signal.

The unique aspects of this thesis are – (a) a search region is defined within which gas bubble signal and systolic phase could exist. This search region is found in the new representation of HS which is very much effective for the Doppler ultrasound signal, more specifically for the high graded Doppler ultrasound signal. - (b) the development of an algorithm called ascending slope tracing algorithm. This algorithm is applied to the time-varying mean frequency for the purpose of signal segmentation on the basis of gas bubble signal characteristics. Despite the variation in gas bubble signal strength this algorithm can detect the segments representing the gas bubble signal. - (c) the gas bubble detection based on fuzzy logic rule. Using different threshold values for different parameters is very difficult for making a meaningful decision for the gas bubble signal detection in the field of medical diagnosis. Hence membership values are used instead of threshold values for all the parameters. Then the gas bubble detection results are defined precisely in terms of membership value.

7.2 Future directions

In this thesis, a number of algorithms are developed and all of these algorithms are dependent on the EMD method. At first, instantaneous amplitude, instantaneous phase and IF is obtained by applying the DHT method to the IMFs. These IMFs are obtained through the decomposition of the signal using EMD method. Then, HS is generated using instantaneous amplitude and IF. Time-varying mean frequency is derived using instantaneous amplitude and IF. Moreover, all the parameters in time-varying mean frequency domain and IMF-based time domain are determined on the basis of EMD method. Therefore, it is evident that all the algorithms are exploiting EMD method in any way. Improving the EMD method could push the whole process from different angles. Hence, further improvement is expected in EMD method by implementing the EMD process as a perceptually tuned filter bank instead of simple EMD. Ensemble empirical mode decomposition (EEMD) could be an alternative to the simple EMD method. EEMD is used to resolve the mode mixing problem of EMD. Turning tangent empirical mode decomposition (2T-EMD) could be another alternative to the EMD method. Efficient representation of the HS could be given through the generation of a huge number of IMF using 2T-EMD method.

Some well-known parameters are determined from the segments in time-varying mean frequency domain and IMF-based time domain in this study. Discovering signal

dependent gas bubble signal characteristics and utilizing those characteristics in the signal segmentation algorithm could provide better accuracy in the extraction of the segments representing gas bubble signals. More sensitive parameters should be extracted and exploited to the gas bubble signal detection to make the detection process very much effective.

It is easily perceived that the proposed algorithms can detect the gas bubbles for grade I, II and III signals. However, for grade IV signal our proposed algorithm is not adequate. More advanced algorithm is required to the detection of grade IV gas bubble signals. The automatic detection of search region for all the grades of signals, grade IV gas bubble signal detection and size estimation of gas bubbles for all the grades of signals are the main concern for our future works. Furthermore, there is no reported physiological meaning for IMFs regarding gas bubble signal. This is a research area that should be pursued in the future.

REFERENCES

[1] C. M. S. Muth, Eric S., “Gas embolism”, New England journal of medicine, vol. 342, no. 7, pp. 476-482, 2000.

[2] M. P. Spencer, S. D. Campbell, and J. L. Lindbergh, “Experiments on decompression bubbles in the circulation using ultrasonic and electromagnetic flowmeters”, J. Occupational Med., vol. 11, no. 5, pp. 238-244, 1969.

[3] G. L. Kelly, G. Dodi, and B. Eisman, “Ultrasound detection of fat emboli”, Surg. Forum, vol. 23, pp. 459-461, 1972.

[4] M. P. Spencer, G. I. Thomas, S. C. Nicholls, and L. R. Sauvage, “Detection of middle cerebral artery emboli during carotid endarterectomy using transcranial Doppler ultrasonography”, Stroke, vol. 21, no. 3, pp. 415-423, 1990.

[5] M. Siebler, M. Sitzer, and H. Steinmetz, “Detection of intracranial emboli in patient with symptomatic extracranial carotid artery disease”, Stroke, vol. 23, no. 11, pp. 1652-1654, 1992.

[6] D. Russell, K. P. Madden, W. M. Clark, P. M. Sandset, and J. A. Zivin, “Detection of arterial emboli using Doppler ultrasound in rabbits”, Stroke, vol. 22, no. 2, pp. 253-238, 1991.

[7] Eric L. Cutler, “Gas embolic factors in cardiovascular health”, Master’s thesis, University of Nebraska-Lincoln, United states, 2011.

[8] Motooki Nose, Isamu Harao, Michishige Kono, Yusaku Motoyama, Yoshito Hanyuda, Rikiya Takashima, and Fumio Eda, “Pneumatic deep caisson work using helium mixed gas (Trimix) at the meiko nishi-ohashi west side bridge foundation construction”, Proceedings of the 13th meetings of the united states-japan cooperative program in natural resources, pp. 25-32, 1995.

[9] Odd Arnold Kildahl-Andersen, “Production and characterization of monocyte-derived cytotoxic and its role in monocyte-mediated cytotoxicity”.

[10] M. R. Shalaby, “Immunoregulatory properties of the TNF-α and the related cytokines”.

[11] M. P. Spencer, “Decompression limits for compressed air determined by ultrasonically detected blood bubbles”, J. Appl. Phy., vol. 40, no. 2, pp. 229-235, 1976.

[12] J. T. Bushberg, J. A. Seilbert, E. M. Leidholdt, and J. M. Boone, “The Essential Physics of Medical Imaging”, Lippincott Williams and Wilkins, 2002.

[13] Olav Sande Eftedal, “Ultrasonic detection of decompression induced vascular microbubbles”, PhD thesis, Faculty of medicine, Norwegian university of science and technology, 2007.

[14] Emmanuel Roy, Silvio Montresor, Pierre Abraham, and Jean-Louis Saumet, “Spectrogram analysis of arterial doppler signals for off-line automated HITS detection”, Ultrasound Med. Biol., vol. 25, no. 3, pp. 349-359, 1999.
[15] Emmanuel Roy, Pierre Abraham, Silvio Montresor, and Jean-Louis Saumet, “Comparison of time-frequency estimators for peripheral embolus detection”, Ultrasound Med. Biol., vol. 26, no. 3, pp. 419-423, 2000.
[16] K. Kisman, “Spectral analysis of Doppler ultrasonic decompression data”, Ultrasonics, vol. 15, no. 3, pp. 105-110, 1977.
[17] H. Markus, M. Cullinane, and G. Reid, “Improved automated detection of embolic signals using a novel frequency filtering approach”, Stroke, vol. 30, no. 8, pp. 1610-1615, 1999.
[18] M. Cullinane, G. Reid, R. Dittrich, Z. Kaposzta, R. Ackerstaff, V. Babikian, D. W. Droste, D. Grosset, M. Siebler, L. Valton, and H. S. Markus, “Evaluation of new online automated embolic signal detection algorithm, including comparison with panel of international experts”, Stroke, vol. 31, no. 6, pp. 1335-1341, 2000.
[19] N. Aydin, S. Padayachee, H. S. Markus, “The use of wavelet transform to describe embolic signals”, Ultrasound Med. Biol., vol.25, no. 6, pp.953-958, 1999.
[20] Brian S. Krongold, Akbar M. Sayeed, Mark A. Moehring, James A. Ritcey, Merrill P. Spencer and Douglas L. Jones, “Time-scale detection of microemboli in flowing blood with Doppler ultrasound ”, IEEE Trans. Biomed. Eng., vol. 46, no. 9, pp. 1081-1089, 1999.
[21] D. L. Jones and R. G. Baraniuk, “Efficient approximation of continuous wavelet transforms ”, Electron. Lett., vol. 27, no. 9, pp. 748-750, 1991.
[22] Nizamettin Aydin, Farokh Marvasti and Hugh S. Markus, “Embolic Doppler ultrasound signal detection using discrete wavelet transform”, IEEE Transactions on Information Technology in Biomedicine, vol. 8, no. 2, pp. 182-190, 2004.
[23] Ping-Wing Lui, Brent C. B. Chan, Francis H. Y. Chan, Paul W. F. Poon, Hsin Wang, and F. K. Lam, “Wavelet analysis of embolic heart sound detected by precordial Doppler ultrasound during continuous venous air embolism in dogs”, Anesthesia and Analgesia, vol. 86, no. 2, pp. 325-331, 1998.
[24] M. A. Chappell and S. J. Payne, “A method for the automated detection of venous gas bubbles in humans using empirical mode decomposition”, Annals of Biomedical Engineering, vol. 33, no. 10, pp. 1411-1421, 2005.
[25] P. Hamilton and W. Tompkins, “Quantitative investigation of QRS detection rules using the MIT/BIH arrhythmia database”, IEEE Trans. Biomed. Eng., vol. 33, no. 12, pp. 1157-1165, 1986.
[26] Jean-Marc Girault, Denis Kouame, Abdeldjalil Ouahabi and Frederic

Patat, ”Micro-emboli detection: an ultrasound doppler signal processing viewpoint”, IEEE Trans. Biomed. Eng., vol. 47, no. 11, pp. 1431-1439, 2000.
[27] Takayoshi Nakai, Masahiro Watanabe and Hisayoshi Suzuki, “Use of a linear predictive analysis method to detect gas bubbles generated in the bloodstream during decompression”, Systems and computers in Japan, vol. 24, no. 6, pp. 60-71, 1993.
[28] M. P. Spencer., “Decompression limits for compressed air determined by ultrasonically detected blood bubbles”, J. Appl. Phys., vol. 40, no. 2, pp. 229-235, 1976.
[29] M. A. Chappell and S. J. Payne, “A method for the automated detection of venous gas bubbles in humans using empirical mode decomposition”, Annals of Biomedical Engineering, vol. 33, no. 10, pp. 1411-1421, 2005.
[30] Z. E. Hadj Slimane and A. Nait-Ali, “QRS complex detection using empirical mode decomposition”, Digital Signal Processing, vol. 20, no. 4, pp. 1221-1228, 2010.
[31] N. E. Huang, Z. Shen, S. R. Long, M. C. Wu, H. H. Shih, Q. Zheng, N. -C. Yen, C. C. Tung, and H. H. Liu, “The empirical mode decomposition and the Hilbert spectrum for nonlinear and non-stationary time series analysis”, Proc. Roy. Soc. of London, vol. 454, no. 1971, pp. 903-995, 1998.
[32] P. Flandrin, G. Rilling and P. Gonqalves, “Empirical mode decomposition as a filter bank”, IEEE Signal Processing Letters, vol. 11, no. 2, pp. 112-114, 2004.
[33] B. Z. Wu and N. E. Huang, “A study of the characteristics of white noise using empirical mode decomposition method”, Proc. Roy. Soc. of London, vol. 460, no. 2046, pp. 1597-1611, 2004.
[34] M. K. I. Molla and K. Hirose, “Single-mixture audio source separation by subspace decomposition of hilbert spectrum”, IEEE Transactions on Audio, Speech and Language Processing, vol. 15, no. 3, pp. 893-900, 2007.
[35] N. E. Huang, M. –L. Wu, W. Qu, S. R. Long and S. S. P. Shen, “Application of Hilbert-Huang transform to non-stationary financial time series analysis”, Applied Stochastic Model in Business and Industry, vol. 19, no. 3, pp. 245-268, 2003.
[36] S. A. Taouli and F. Bereksi-Regig, “Detection of QRS complexes in ECG signals based on empirical mode decomposition”, Global Journal of Computer Science and Technology, vol. 11, no. 20, pp. 10-17, 2011.
[37] M. Aboy, J. McNames, T. Thong, D. Tsunami, M. S. Ellenby and B. Goldstein, “An automatic beat detection algorithm for pressure signals”, IEEE Transactions on Biomedical Engineering, vol. 52, no. 10, pp. 1662-1670, 2005.
[38] M. L. Schmidt, L. Johannesen, J. S. Sorensen, K. Lundhus, S. E. Schmidt and N. H. Staalsen, “Detection of systole and diastole start in cardiac and arterial pressure recordings”, Computing in Cardiology, pp. 381-384, Belfast, Northern Ireland, September 26-29, 2010.

[39] W. Zong, T. Heldt, G. B. Moody and R. G. Mark, “An open-source algorithm to detect onset of arterial blood pressure pulses”, Computing in Cardiology, pp. 259-262, Thessaloniki Chalkidiki, Greece, September 21-24, 2003.
[40] Leon cohen, “Time-frequency analysis”, Prentice hall PTR, Upper saddle river, New jersy.
[41] S. Olhede, and A. T. Walden, “The Hilbert spectrum via wavelet projections”, Proceedings of the royal society A mathematical physical and engineering sciences, vol. 460, no. 2044, pp. 955-975, 2004.
[42] M. A. Moehring and J. R. Keppler, “Pulse Doppler ultrasound detection, characterization and size estimation of emboli in flowing blood”, IEEE Trans. Biomed. Eng., vol. 41, no. 1, pp. 35-44, 1994.
[43] Teng Wang, Yuanyuan Wang, “Optimization of pulsed Doppler sample volume for emboli detection”, International conference on bioinformatics and biomedical engineering, pp. 1-4, Wuhan, May 10-12, 2011.
[44] Nebuya S, Noshiro M, Brown BH, Smallwood RH, Milnes P, “Estimation of the size of air emboli detectable by electrical impedance measurement”, Medical and biological engineering and computing, vol. 42, no. 1, pp. 142-144, 2004.
[45] Da Xu, Yuanyuan Wang, “An automated feature extraction and emboli detection system based on the PCA and fuzzy sets”, Elsevier, Computers in biology and medicine, vol. 37, no. 6, pp. 861-871, 2007.
[46] D. H. Evans, J. L. Smith, A. R. Naylor, “Characteristics of Doppler ultrasound signals recorded from cerebral emboli”, Ultrasound in Med. and Biol., vol. 23, no. 1, pp. 140-140(1), 1997.
[47] R. Y. Nishi, “The scattering and absorption of sound waves by a gas bubble in a viscous liquid”, Acoustica, vol. 33, no. 2, pp. 65-74, 1975.
[48] L. A. Zadeh, “Fuzzy sets”, Information and control, vol. 8, no. 3, pp. 338-353, 1965.

List of publications

(related to the thesis work)

Journal paper

1. Md. Iqbal Aziz Khan, Md. Ekramul Hamid and Takayoshi Nakai, "Systolic phase detection from pulsed Doppler ultrasound signal using EMD-DHT based approach", International Journal of Signal Processing, Image Processing and Pattern Recognition, Vol. 7, No. 5, pp. 207-216, 2014.

International conference paper

1. Md. Iqbal Aziz Khan, Md. Ekramul Hamid and Takayoshi Nakai, "EEMD and DHT based solution to detect systolic phase from Doppler ultrasound signal", International conference on materials, electronics and information engineering, ICMEIE-2015, University of Rajshahi, Bangladesh, June 5-6, 2015
2. Md. Iqbal Aziz Khan, Md. Ekramul Hamid and Takayoshi Nakai, "2T-EMD and DHT based approach to systolic phase detection from Doppler ultrasound signal", The 22nd international congress on sound and vibration, ICSV22, Plazzo dei congress, Florence, Italy, July 12-16, 2015

International meetings

1. Md. Iqbal Aziz Khan and Takayoshi Nakai, "Empirical mode decomposition-discrete Hilbert transform based solution to detect decompression-induced gas bubble from Doppler ultrasound signal", The journal of the acoustical society of America, Vol. 137, No. 4, April 2015, 169th meeting of the acoustical society of America.

National conference papers/symposiums

1. Md. Iqbal Aziz Khan and Takayoshi Nakai, "Spectral component analysis to detect gas bubbles in the bloodstream", Acoustical society of Japan, March, 2013.
2. Md. Iqbal Aziz Khan and Takayoshi Nakai, "Gas bubble detection in the bloodstream using empirical mode decomposition-systolic phase detection", Acoustical society of Japan, September, 2013.

3. Md. Iqbal Aziz Khan and Takayoshi Nakai, “Systolic phase detection from Doppler ultrasound using empirical mode decomposition“, Acoustical society of Japan, March, 2014.
4. Md. Iqbal Aziz Khan and Takayoshi Nakai, “A new approach to detect systolic phase from Doppler ultrasound“, Acoustical society of Japan, September, 2014.
5. Md. Iqbal Aziz Khan and Takayoshi Nakai, “EMD-HT based decompression induced gas bubble detection from Doppler ultrasound signal”, Acoustical society of Japan, March, 2015.
6. Md. Iqbal Aziz Khan and Takayoshi Nakai, “Empirical mode decomposition based systolic phase detection from Doppler ultrasound”, The 15th Takayanagi Kenjiro memorial symposium, pp. s4-26-1: s4-26-5, Shizuoka University, Japan, 2013.